

Final Report for DE-FG02-02ER45983

Recipient: Johns Hopkins University

Project Title: Pulsed Neutron Scattering Studies of Strongly Fluctuating solids

Principal Investigator: Collin Broholm

Team Members: Toby Perring (ISIS facility contact), Joost van Duijn (Post doctoral fellow), Seth Jonas (Graduate Student)

Executive Summary

The conventional description of a solid is based on a static atomic structure with small amplitude so-called harmonic fluctuations about it. This project has explored materials where fluctuations are sufficiently strong to severely challenge this approach and lead to unexpected and potentially useful materials properties. Fluctuations are enhanced when a large number of configurations share the same energy. We used pulsed spallation source neutron scattering to obtain detailed microscopic information about structure and fluctuations in such materials. The results enhance our understanding of strongly fluctuating solids and their potential for technical applications. Because new materials require new experimental techniques, the project has also developed new techniques for probing strongly fluctuating solids. Examples of material that were studied are ZrW_2O_8 with large amplitude molecular motion that leads to negative thermal expansion, NiGa_2S_4 where competing interactions lead to an anomalous short range ordered magnet, $\text{Pr}_{1-x}\text{Bi}_x\text{Ru}_2\text{O}_7$ where a partially filled electron shell (Pr) in a weakly disordered environment produces anomalous metallic properties, and TbMnO_3 where competing interactions lead to a magneto-electric phase. The experiments on TbMnO_3 exemplify the relationship between research funded by this project and future applications. Magneto-electric materials may produce a magnetic field when an electric field is applied or vice versa. Our experiments have clarified the reason why electric and magnetic polarization is coupled in TbMnO_3 . While this knowledge does not render TbMnO_3 useful for applications it will focus the search for a practical room temperature magneto-electric for applications.

Objectives versus accomplishments

The general objectives laid out in the proposal were accomplished though sometimes through research on different materials than initially planned. This is typical for a scientific project of this nature in order to respond to developments and opportunities that could not be anticipated while preparing the funding proposal. ZrW_2O_8 was part of the original proposal and we made significant progress towards understanding its anomalous thermal contraction. A paper is still being prepared to describe some of the neutron scattering results from this compound. TbMnO_3 was not part of the original proposal because its unusual magneto-electric properties had not been discovered at that point. Our work under this project uncovered the mechanism behind magneto-electricity in this material and indeed in an entire class of oxides namely magnetic inversion symmetry breaking. Examples of proposed projects that ultimately did not lead to publications were attempts to probe spin singlet formation in MgTi_2O_4 and spin waves in CrO_2 . In both

cases the experiments turned out not to be feasible on present day instrumentation and with currently available samples. However, the experience gained paves the way for future experiments using advanced instrumentation of the US spallation neutron source. In place of these projects we reached a comprehensive understanding of apparent heavy fermion behavior in $\text{Pr}_{1-x}\text{Bi}_x\text{Ru}_2\text{O}_4$. This anomalous heavy fermion like metal was discovered by colleagues at Rutgers University during the project. By moving rapidly using advanced pulsed neutron instrumentation at ISIS, we were able to include a full explanation of this material in the Physical Review Letter that also reported its discovery. This is an unusual accomplishment consistent with the project goal of contributing to the early stages of materials development through neutron scattering.

Summary of Project Activities

NiGa₂S₄ While neutron scattering is often the ultimate tool for elucidating atomic scale structure and dynamics, the complexity of the experiments has sometimes limited early impact in the materials development cycle. Our experiments on NiGa₂S₄ are an exception to this. Through collaboration with Dr. Satoru Nakatsuji and Prof. Y. Maeno who embody a leading materials synthesis group at Kyoto University in Japan, we have been fortunate to work on a very interesting new material. NiGa₂S₄ is a triangular lattice spin-1 antiferromagnet with unusual bulk properties indicating that there might be something new for us to learn about cooperative effects in this basic physical system. The specific heat shows two maxima versus temperature none of which indicate a phase transition to long range magnetic order. This is very unusual for a Bravais lattice with no apparent disorder. Our pulsed neutron scattering experiments carried out at the NIST Center for Neutron Research

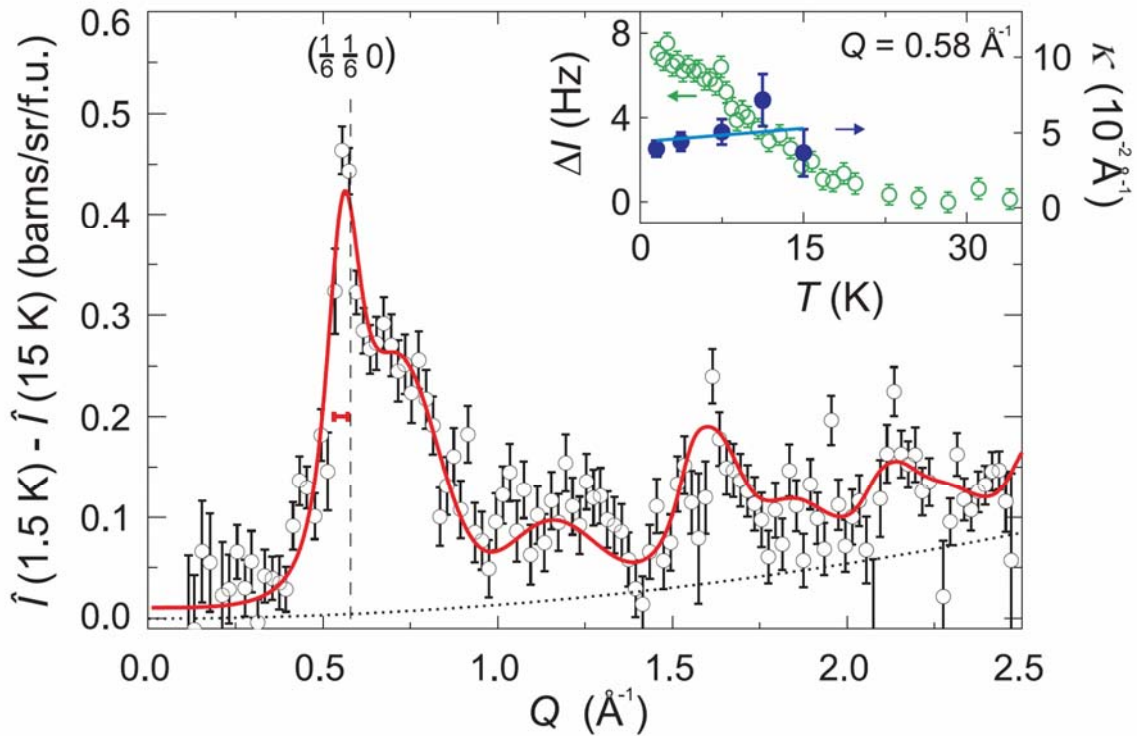


Figure 1. Elastic magnetic neutron scattering from NiGa_2S_4 at $T=1.4$ K. The solid line was calculated for a short range ordered incommensurate spin structure as indicated in Fig. 2.

Neutron research revealed what may be the key to understanding the anomalous quantum magnetism of this material. The key data are shown in Fig. 1. The Q -dependent low temperature elastic scattering shows nano-scale quasi-static correlations with half the characteristic wave vector compared to our initial expectations. The corresponding real space spin structure is indicated in fig. 2. A possible explanation for the incommensurate structure is competing first and third neighbor spin interactions in this material. Indeed, consideration of the local coordination in the NiS_2 layer indicates that this is a strong possibility. The interesting aspect of this work is that a spin disordered state with strong fluctuations has been identified in a frustrated magnet on an apparently perfectly ordered crystalline Bravais lattice. If this material can be made conducting through doping (not unlikely given the similarities to the cobaltate superconductor and NiS_2) one might expect highly non-trivial metallic properties. Our manuscript is now under consideration for publication as a letter to *SCIENCE*. We are also in the process of carrying out neutron measurements on single crystalline samples to obtain a deeper understanding of interactions and correlations in this remarkable new material.

TbMnO_3 has attracted considerable recent attention because of a coincident magnetic and ferro-electric phase transition that occurs at $T=27$ K. We carried out a comprehensive investigation of the magnetic structure in the magneto-electric phase using a four circle neutron diffractometer at the Paul Scherrer institute in Switzerland. The experiment pinpointed the distinguishing feature of the magneto-electric phase as being the lack of a center of inversion. By breaking spatial inversion symmetry and by virtue of magneto-elastic coupling, the incommensurate ordered structure acts as an effective electric field

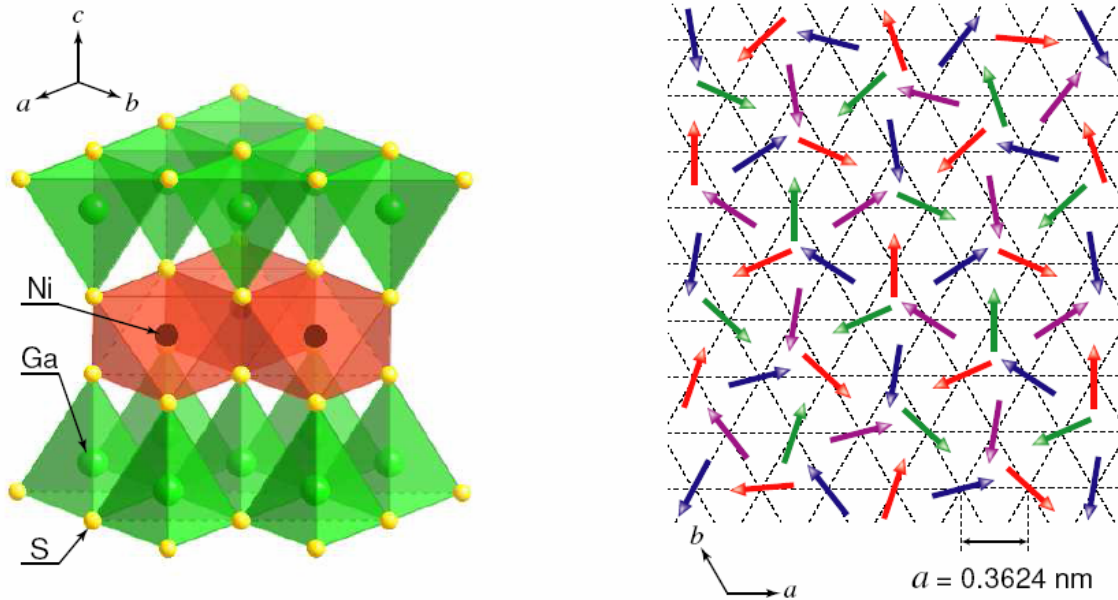


Figure 2. Left figure shows the crystal structure of NiGa_2S_4 . A relatively simple layered compound that contains an exact triangular lattice plane of spin-1 nickel atoms. The right figure indicates the incommensurate nano-scale spin order that was detected through pulsed elastic neutron scattering at the NIST Center for neutron research.

on the insulating material. The result is magnetically driven electric polarization. This result has been submitted to Physical Review Letters for publication.

A comprehensive understanding of magneto-elasticity and ideas on how to increase the critical temperature towards room temperature for applications, however, requires knowledge of the relevant interactions. This information can be obtained from inelastic magnetic neutron scattering experiments. Large single crystals were prepared for this purpose by Prof. S.-W. Cheong et al. at Rutgers University and co-mounted in an 18 g mosaic on a time of flight diffractometer at the ISIS facility. The inelastic experiment was carried out on the MAPS spectrometer at ISIS. We used a novel “step-scan” technique for time of flight inelastic neutron scattering that we pioneered for ZrW_2O_8 in the previous funding period. The result is a spectacular set of data probing inelastic scattering in a four dimensional \mathbf{Q} -E volume. Two slices through this huge data-set are presented in Figure 3. In my view these data represent a quantum leap in inelastic neutron scattering. Whereas in the past such experiments had to focus on measuring dispersion relations along high symmetry directions, our measurements, carried out in only 10 days, show that it is now possible to map inelastic scattering throughout the Brillouin zone. With SEQUOIA and ARCS at the SNS such measurements may in fact become routine! TbMnO_3 is a particularly good test case as it is a topical material and the incommensurate structure necessitates a comprehensive data set. We plan to work with a theoretical group to develop a model that can link exchange constants to inelastic scattering so we can extract unbiased information about interactions and spin excitations in this incommensurate orbitally ordered transition metal oxide.

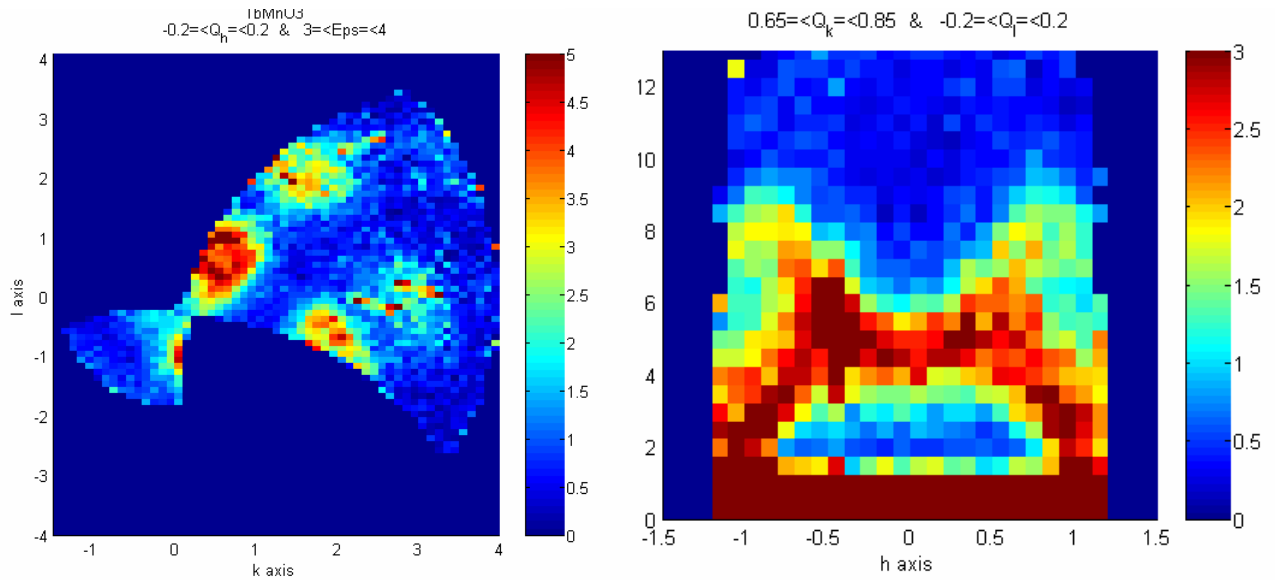


Figure 3. Two slices through a complete measurement of the \mathbf{Q} -E dependent inelastic magnetic neutrons scattering spectrum in magneto-electric TbMnO_3 . These are fully resolved data covering several Brillouin zones in a three dimensional orthorhombic solid.

Pyrochlore magnets display a vast range of interesting physical effects related to geometrical frustration and weak connectivity. As opposed to more conventional antiferromagnets where near neighbor antiferromagnetic interactions select a specific long range ordered state, these interactions only define a low energy manifold on a pyrochlore lattice. The situation becomes particularly interesting for metallic systems as strong fluctuations in the low energy manifold can have qualitative effects on charge transport and thermodynamic properties. Our inelastic scattering experiments on pyrochlore $\text{Pr}_{1-x}\text{Bi}_x\text{Ru}_2\text{O}_7$ revealed a novel effect wherein a non-Kramers doublet ground state undergoes inhomogeneous level splitting due to a distribution of electro-static environments. We combined bulk measurements with inelastic scattering data to reach a comprehensive understanding of the anomalous properties of this alloy. Figure 4 shows that we were able to calculate temperature dependent specific heat and susceptibility data from inelastic neutron scattering data with no truly adjustable parameters. The results were recently published in Physical Review Letters.

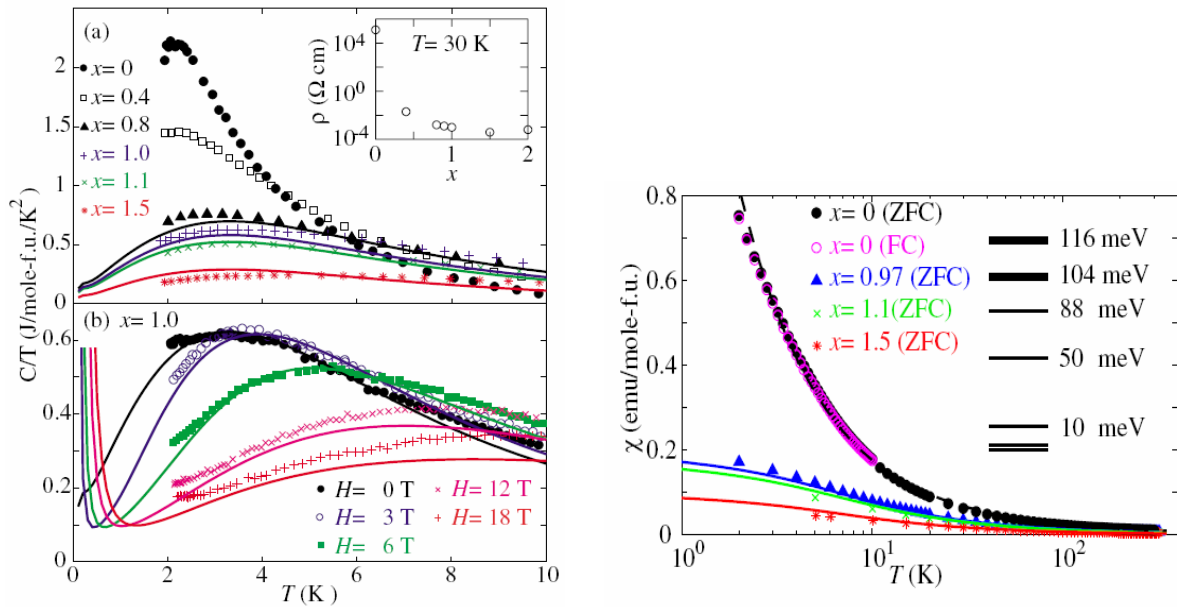


Figure 4. Specific heat and susceptibility data for the pyrochlore antiferromagnet $\text{Pr}_{1-x}\text{Bi}_x\text{Ru}_2\text{O}_7$, which contains non-Kramers Pr ions in an inhomogeneous environment. The solid lines were calculated on the basis of inelastic neutron scattering data from the IRIS instrument at ISIS. The good agreement between calculations and bulk data indicate that our interpretation in terms of inhomogeneous level splitting of a non-Kramers ion is correct. The results were recently published in Phys. Rev. Lett.

Our experiments on $\text{Y}_2\text{Ru}_2\text{O}_7$ provide a simple example of a strong coupling magnetic phase transition possibly brought about through magneto-elastic effects. We have developed an elegant way of analyzing the powder inelastic neutron scattering data that enables extraction of a local spin fluctuation rate without unfounded assumptions and taking advantage of the full data set from a modern time of flight spectrometer such as MARI at ISIS. Fig. 5 shows the main result of the experiment which is the development of a resonance like feature in the spectrum below the antiferromagnetic phase transition. There are strong similarities to the spinel antiferromagnet ZnCr_2O_4 both in the energy and wave vector dependence of this resonance, which is important as it indicates that we have

identified a generic feature of frustrated magnetism. A preprint is being edited for submission to Phys. Rev. B.

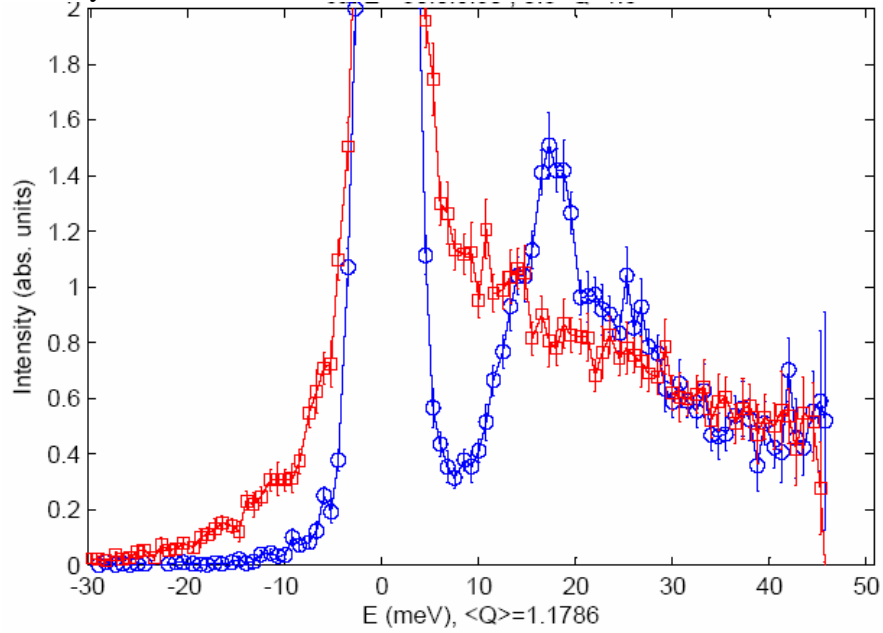


Figure 4. Magnetic excitation spectrum of $\text{Y}_2\text{Ru}_2\text{O}_7$ at $T=1.5$ K and at $T=90$ K which is below and above the Néel temperature of $T_N=80$ K. Long range magnetic order causes the development of a well defined spin resonance at an energy of approximately 19 meV.

ZrW₂O₈ is an insulating oxide that exhibits isotropic thermal contraction over a temperature range from the absolute zero to well above room temperature. Key to understanding this anomalous and potentially useful behavior is lattice dynamics. We therefore carried out a comprehensive neutron scattering study of phonon scattering in ZrW_2O_8 using inelastic neutron scattering. Graduate student Seth Jonas has now developed software for analysis and display of the large data set that was collected. We plan to publish these results along with an ab-initio calculations of the inelastic neutron scattering cross section as a way to validate or refute the latter. This work is important as it will establish whether novel cooperative effects are needed to understand negative thermal expansion or whether the effect is contained in standard anharmonic phonon theory.

Joost Van Duijn grew large single crystals of ZrW_2O_8 in collaboration with Glen Kowach for these neutrons scattering experiments (See Fig. 5). These crystals also enabled resonant ultrasound spectroscopy to measure the elastic constants versus temperature. A paper describing these results was published in Physical Review Letters.

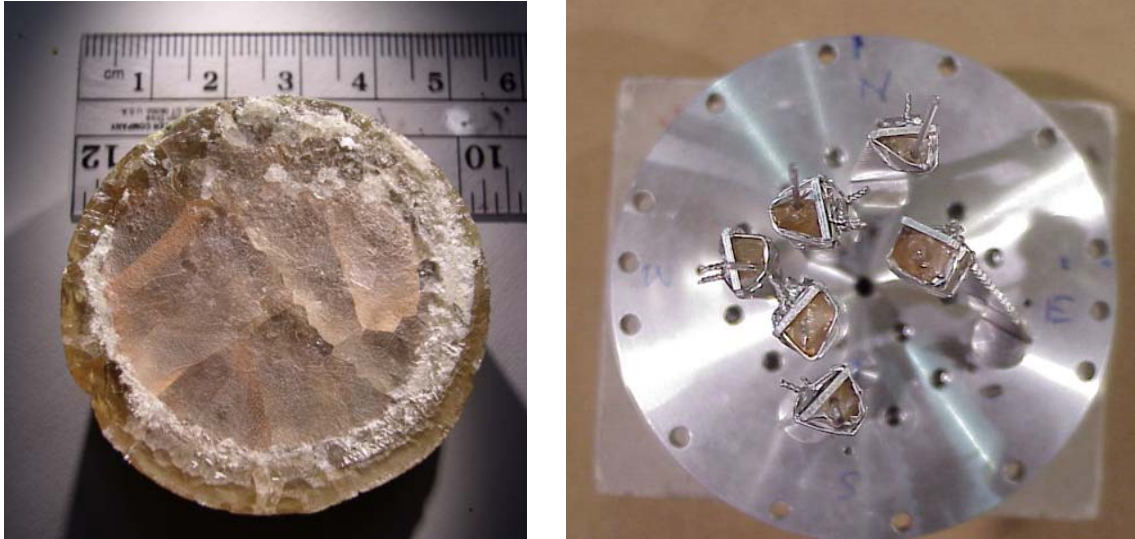


Figure 5. Synthesis and alignment of ZrW_2O_8 single crystalline samples. Left frame shows a boule of material after removal from the high temperature furnace. There are clear indications of large single crystalline samples close to the surface. Right frame shows 6 pre-aligned samples just prior to carrying out the final alignment at NIST. The thin aluminum pins pointing out of the picture indicate the (001) direction as determined on SXD.

Singlet formation in a spin-1/2 spinel antiferromagnet: MgTi_2O_4 shows a weakly temperature independent magnetic susceptibility in an extended temperature range below room temperature. The only feature is a step like reduction in susceptibility with temperature at $T=260$ K and a Curie tail at the lowest temperatures that accounts for just 3% of the Ti^{3+} sites. These results are surprising since every Ti^{3+} site should carry a spin-1/2 degree of freedom and give rise to Curie-Weiss behavior with the corresponding effective moment. The hypothesis that we worked from was and remains that spin-1/2 degrees of freedom form some type of cooperative singlet state. Indeed there are theoretical predictions that this should happen for spin-1/2 on a lattice of corner-sharing tetrahedral. A high temperature susceptibility measurement carried out by a graduate student on the project (Seth Jonas) provides support for this interpretation as the susceptibility is found to increase well above room-temperature. The best evidence for singlet formation would however be observation through neutron scattering of the corresponding singlet-triplet excitations. We therefore performed an inelastic neutron scattering experiment on a powder sample using the MARI instrument at ISIS. The experiment showed inelastic scattering in the relevant range of energies, however, it was not possible to establish the relative composition of phonon and magnetic neutron scattering. Given the tetragonal distortion that occurs at $T=260$, it is quite likely that MgTi_2O_4 has strong magneto-elastic effects and that the elementary excitations have a vibrational and magnetic component. To separate these we believe the best approach is inelastic neutron scattering from a single crystalline sample. These experiments however, could not be carried out under this project because they await progress in growing large single crystals of this substance.

Product Developed Under the Award

Published papers (the publications are attached to this document)

1. “Unconventional Magnetic Correlations in DyB₂C and HoB₂C studied by μ SR”, J. van Duijn, A. D. Hillier, R. Watanuki, K. Suzuki, J. P. Attfield, *Physica B* **378-380**, 477 (2006).
2. “Metallic spin-liquid behavior of the geometrically frustrated Kondo lattice Pr₂Ir₂O₇”, S. Nakatsuji, Y. Machida, Y. Maeno, T. Tayama, T. Sakakibara, J. van Duijn, L. Balicas, J. N. Millican, R. T. Macaluso, J. Y. Chan, *Phys. Rev. Lett.* **96**, 087204 (2006).
3. “Spin Disorder on a Triangular Lattice”, Satoru Nakatsuji, Yusuke Nambu, Hiroshi Tonomura, Osamu Sakai, Seth Jonas, Collin Broholm, Hirokazu Tsunetsugu, Yiming Qiu, and Yoshiteru Maeno, *Science* **309**, 1697 (2005).
4. “Magnetic Inversion Symmetry Breaking and Ferroelectricity in TbMnO₃” M. Kenzelmann, A. B. Harris, S. Jonas, C. Broholm, J. Schefer, S. B. Kim, C. L. Zhang, S.-W. Cheong, O. P. Vajk, and J. W. Lynn, *Phys. Rev. Lett.* **95**, 087206 (2005).
5. “Inhomogeneous Level Splitting in Pr_xBi_{2-x}Ru₂O₇”, J. van Duijn, K. H. Kim, N. Hur, D. Adroja, M. A. Adams, Q. Z. Huang, M. Jaime, S.-W. Cheong, C. Broholm, and T. G. Perring, *Phys. Rev. Lett.* **94**, 177201 (2005).
6. “Crystalline electric field levels and magnetic properties of the metallic pyrochlore compound Pr₂Ir₂O₇”, Y. Machida, S. Nakatsuji, H. Tonomura, T. Tayama, T. Sakakibara, J. van Duijn, C. Broholm, Y. Maeno, *J. Phys. Chem. Sol.* **66**, 1435 (2005).
7. “Monocrystal elastic constants of the negative-thermal-expansion compound zirconium tungstate (ZrW₂O₈)” F. R. Drymiotis, H. Ledbetter, J. B. Betts, T. Kimura, J. C. Lashley, A. Migliori, A. P. Ramirez, G. Kowach, J. Van Duijn, *Phys. Rev. Lett.* **93**, 025502 (2004).

Papers in preparation (these papers will appear with DoE acknowledgement)

1. “Evidence for a Strong Coupling Transition in the Frustrated Pyrochlore System Y₂Ru₂O₇”, J. van Duijn, N. Hur, J. W. Taylor, Y. Qiu, Q. Z. Huang, S.-W. Cheong, C. Broholm, and T. G. Perring, preprint intended for *Phys. Rev. B* (2006).
2. “Spin Waves and Magnetic Interactions in TbMnO₃”, J. van Duijn, S. Jonas, T. G. Perring, C. Broholm, S. B. Kim, C. L. Zhang, S.-W. Cheong, in preparation for *Phys. Rev. B*. (2006).

3. "Low Energy Phonons in a Material with Negative Thermal Expansion: ZrW_2O_8 ", J. van Duijn, G. Lawes, T. G. Perring, and C. Broholm, in preparation for Phys. Rev. B (2006).
4. "Heavy Fermion Behavior in a Dilute Frustrated Magnet", J. van Duijn, K. H. Kim, N. Hur, D. Adroja, M. Adams, F. Fernandez-Alonso, Q. Z. Huang, S.-W. Cheong, C. Broholm, and T.G. Perring, in preparation for Phys. Rev. B (2006).
5. "Unusual compressibility in the negative-thermal-expansion material ZrW_2O_8 ", C. Pantea, A. Migliori, P. B. Littlewood, Y. Zhao, H. Ledbetter, T. Kimura, J. Van Duijn, G. R. Kowach, submitted to Nature (2005).

Invited Talks

Viewgraphs are available at

<http://www.pha.jhu.edu/~broholm/homepage/seminarsandtalks.htm>

1. "Level Splitting and frustration in Metallic pyrochlore systems", Department of Physics and Astronomy, Birmingham University, UK, March 3 (2006).
2. "Magnetic Surprises on a Triangular Lattice", Condensed Matter Physics Seminar, Rutgers University, November 15 (2005).
3. "Inhomogeneous Level Splitting in $\text{Pr}_{1-x}\text{Bi}_x\text{Ru}_2\text{O}_7$ ", Paul Scherrer Institute, Switzerland, December 3, (2004).
4. "Frustrated Magnetism in 2D", Workshop on Strongly Correlated Electron Systems, University of Kentucky, April 24-26, (2005).
5. "Glassy Phases in Two Dimensional Quantum Magnets", Workshop on Quantum Critical Phenomena, Kavli Institute for Theoretical Physics, March 29 and April 1, (2005).
6. "Level Splitting and frustration in Metallic pyrochlore systems", Van der Waals-Zeeman Insitute, Universiteit van Amsterdam, NL, November 12 (2004).
7. "Level Splitting in Frustrated non-Kramers Doublet Systems", International Workshop on Frustrated Magnetism, Montauk Yacht Club, Long Island, NY September 13-17 (2004).
8. "Frustrated Magnetism and Heavy Fermions", at conference on Strongly Correlated Electron Systems, Karlsruhe, Germany, July 29 (2004).

Contributed Talks

1. "Neutron Scattering from a spin-1 triangular lattice antiferromagnet", S. Jonas, APS March Meeting, Baltimore, MD March (2006).
2. "Crystal Field Excitations in a Frustrated Heavy Fermion System, $\text{Pr}_{1.2}\text{Bi}_{0.8}\text{Ru}_2\text{O}_7$ ", J. van Duijn, APS March Meeting, Montreal March (2004).
3. "Crystal Field Excitations in a Frustrated Heavy Fermion System, $\text{Pr}_{1.2}\text{Bi}_{0.8}\text{Ru}_2\text{O}_7$ "; J. van Duijn, at 2004 APS March Meeting, Montreal, Quebec, Canada.
4. "Spin Freezing and Ferromagnetic Cluster Formation in LiNiO_2 "; J. van Duijn at 2003 APS March Meeting, Austin, Texas.

Software Development: Toby Perring, Joost van Duijn, and Seth Jonas have developed a program called HORACE for analysis of very large data sets from a chopper spectrometer such as MAPS at ISIS. The program can handle multiple sample orientations as required for a full sampling of four dimensional scattering space. The program is being used for the analysis of TbMnO_3 and ZrW_2O_8 data and in the process is also being refined. A public release will occur when the program has matured appropriately and it will acknowledge DoE support.

Networks and Collaborations Established: This project has established a strong collaboration between Toby Perring of ISIS, Collin Broholm of Johns Hopkins University, and Joost van Duijn, now at the University of Madrid in Spain. We continue to collaborate to complete work that was initiated through this project. We also plan future collaborative work on materials science, in particular quantum magnetism, and on neutron scattering instrumentation and methods development. The involvement of the PI in this collaboration with ISIS provided valuable experience that helped him to advise DoE on matters related to neutron scattering in various capacities.

Unconventional magnetic correlations in DyB₂C and HoB₂C studied by μ SR

J. van Duijn^{a,b,1,*}, A.D. Hillier^a, R. Watanuki^c, K. Suzuki^d, J.P. Attfield^e

^aISIS Facility, CCLRC, RAL, Didcot OX11 0QX, UK

^bDepartment of Physics & Astronomy, Johns Hopkins University, Baltimore, MD 21218, USA

^cInstitute for Solid State Physics, University of Tokyo, Kashiwa, Chiba 277-8581, Japan

^dGraduate School of Engineering, Yokohama National University, Yokohama 240-8501, Japan

^eSchool of Chemistry, Edinburgh University, Edinburgh EH9 3JJ, UK

Abstract

Muon measurements have been carried out to probe the magnetic correlations within DyB₂C and HoB₂C. These measurements confirm the presence of two independent magnetic processes in DyB₂C and HoB₂C. The onset of the correlations corresponding to the magnetic random layer phase occurred at higher critical temperatures than expected from neutron diffraction experiments.

© 2006 Elsevier B.V. All rights reserved.

PACS: 71.27.+a; 75.30.-m; 76.75.+i

Keywords: RB₂C; Spin frustration; Magnetic random layer lattice; μ SR

Layered rare-earth borocarbides are of interest due to their low-temperature electronic and magnetic properties. These materials are generally metallic and contain layers of planar π -bonded borocarbide layers sandwiching R³⁺ cations that have localized 4fⁿ configurations. In recent years, the RB₂C₂ family has been studied extensively following the discovery of antiferroquadrupolar ordering in DyB₂C₂ ($T_Q = 24.7$ K) [1,2] and HoB₂C₂ ($T_Q = 5.0$ K) [3].

The related RB₂C family of borocarbides (R = Sc, Y and Tb–Lu) [4] contain sheets of rare-earth ions consisting of fused squares and triangles. This arrangement of the rare-earth-ions in RB₂C is topologically equivalent to the Shastry–Sutherland lattice [5]. We have recently reported on the magnetic properties DyB₂C, HoB₂C and ErB₂C [6,7].

ErB₂C has two-sublattice antiferromagnetic order below $T_N = 16.3$ K. DyB₂C and HoB₂C show a coexistence of a

conventional canted $\mathbf{k} = (000)$ ferromagnetic structure and unconventional magnetic correlations. The conventional phase orders at $T_C = 8.5$ and 7.1 K for DyB₂C and HoB₂C, respectively, with an ordered rare-earth moment (3.3 and 2.94 μ_B , respectively) that is much less than observed for DyB₂C₂ and HoB₂C₂ (8.3 and 7.8 μ_B , respectively) [8]. Suggesting that there are still large magnetic fluctuations present below T_C .

Diffraction peaks from the unconventional correlations appear at low-Q above T_C and are present down to the lowest measured temperature. These low-Q peaks consist of sharp resolution limited and broad asymmetric peaks and can be explained by the formation of a Warren-type magnetic random layer (MRL) lattice. Such a MRL lattice can result from frustration arising from either complex spin–spin interactions or spin–quadrupole interactions that can be present in these materials. Interestingly, not only is this unconventional magnetic phase robust to the ordering of part of the moments into a long-range ordered structure, the low-Q peaks associated with it appear at different critical temperatures. This is highly unusual and suggest that these peaks might not belong to a single magnetic phase. Here, we present μ SR measurements which attempt

*Corresponding author. ISIS Facility, CCLRC, RAL, Didcot OX11 0QX, UK.

E-mail address: j.van.duijn@rl.ac.uk (J. van Duijn).

¹This work was supported by DoE through DE-FG02-02ER45983.

to address the nature of the unconventional correlations observed in HoB₂C and DyB₂C.

Polycrystalline samples of DyB₂C and HoB₂C were prepared by arc melting under pure argon. The samples were remelted several times to ensure homogeneity. ZF- μ SR measurements were made using the MuSR spectrometer at the ISIS pulsed muon facility, in the temperature range of 1.2–250 K. Fig. 1 show typical ZF relaxation spectra observed for HoB₂C at 1.2, 100 and 200 K. At all temperatures, the ZF relaxation spectra are well described by a double exponential decay relaxation function of the form

$$A_0 G_z(t) = A_1 e^{-\lambda_1 t} + A_2 e^{-\lambda_2 t} + a_{bg}, \quad (1)$$

where A_1 , λ_1 and A_2 , λ_2 correspond to fast and slow muon relaxation, respectively, and a_{bg} represents a small time-independent background. Typical fits to the data are shown in Fig. 1. The temperature dependence of the relaxation parameters are shown in Figs. 2 and 3.

Both λ_1 and λ_2 show a peak at 80 and 34 K for DyB₂C and HoB₂C, respectively, which is accompanied by a drop of the initial asymmetries to $\frac{1}{3}$ of its high T value, suggesting the onset of a field on the muon site greater than 600 Gauss. This transition is thought to be associated with the onset of the MRL correlations even though these temperatures are higher than those observed by neutron diffraction [6]. An additional peak is observed in λ_1 corresponding to the T_C of the conventional magnetic phase, while λ_2 confirms the presence of large magnetic fluctuations below T_C .

This experiment confirmed the presence of two independent magnetic processes in DyB₂C and HoB₂C. Correlations associated with the MRL phase appear at higher temperatures than initially expected from the neutron diffraction experiment. This discrepancy between the muon and neutron diffraction measurements can be a result of the different time windows probed by the two techniques. Due to the fast muon relaxation and the pulsed nature of

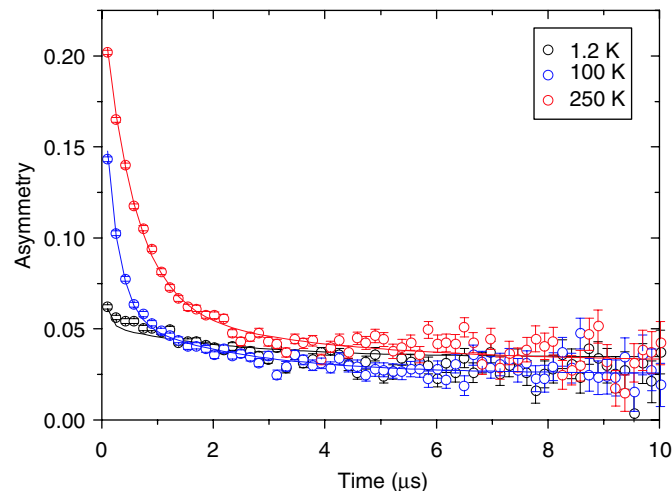


Fig. 1. Typical ZF μ SR spectra of HoB₂C at 1.2 (black), 100 (blue) and 200 (red) K. The solid lines represent fits of Eq. (1) to the data.

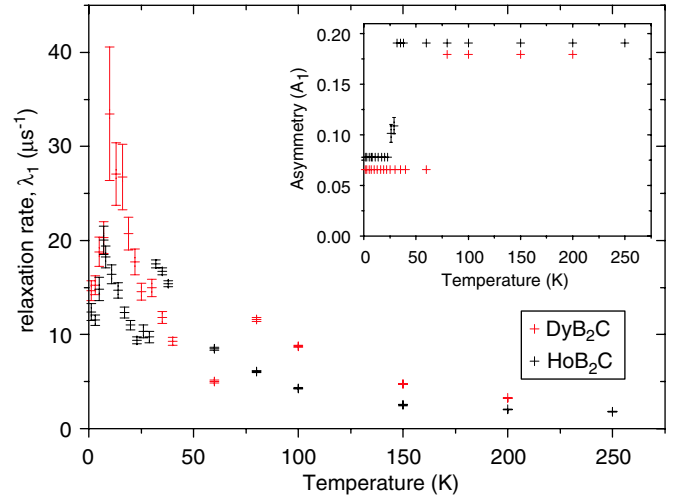


Fig. 2. Temperature dependence of the fast relaxation rate, λ_1 , of DyB₂C (red) and HoB₂C (black). Inset: temperature dependence of the asymmetry, A_1 .

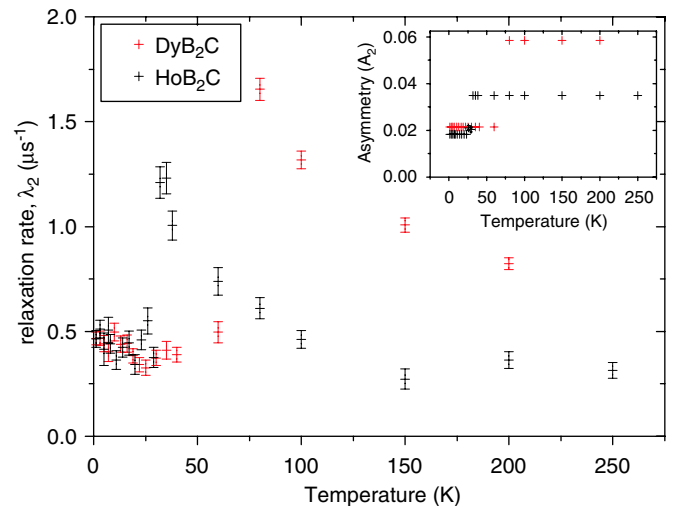


Fig. 3. Temperature dependence of the slow relaxation rate, λ_2 , of DyB₂C (red) and HoB₂C (black). Inset: temperature dependence of the asymmetry A_2 .

the ISIS muon source we were unable to determine the presence of additional transitions within the MRL phase. Additional measurements are underway to probe the detailed nature of the unusual correlations present within these materials.

References

- [1] H. Yamauchi, et al., J. Phys. Soc. Japan 68 (1999) 2057.
- [2] K. Hirota, et al., Phys. Rev. Lett. 84 (2000) 1706.
- [3] H. Onodera, et al., J. Phys. Soc. Japan 68 (1999) 2526.
- [4] J. Bauer, H. Nowotny, Monatshefte für Chemie 102 (1971) 1129; J. Bauer, J. Debuigne, J. Inorg. Nucl. Chem. 37 (1975) 1473; J. Bauer, J. Less. Common Met. 87 (1982) 45.
- [5] B.S. Shastry, B. Sutherland, Physica B 108 (1981) 1069.
- [6] J. van Duijn, et al., Phys. Rev. Lett. 90 (2003) 087201.
- [7] R. Watanuki, et al., Phys. Rev. B 69 (2004) 064433.
- [8] J. van Duijn, et al., Phys. Rev. B 62 (2000) 6410.

Metallic Spin-Liquid Behavior of the Geometrically Frustrated Kondo Lattice $\text{Pr}_2\text{Ir}_2\text{O}_7$

S. Nakatsuji,¹ Y. Machida,¹ Y. Maeno,^{1,2} T. Tayama,³ T. Sakakibara,³ J. van Duijn,⁴ L. Balicas,⁵ J. N. Millican,⁶
R. T. Macaluso,⁶ and Julia Y. Chan⁶

¹Department of Physics, Kyoto University, Kyoto 606-8502, Japan

²International Innovation Center, Kyoto University, Kyoto 606-8501, Japan

³Institute for Solid State Physics (ISSP), University of Tokyo, Kashiwa 277-8581, Japan

⁴ISIS Facility, Rutherford Appleton Laboratory, Chilton, Didcot OX11 0QX, United Kingdom

⁵National High Magnetic Field Laboratory (NHMFL), Tallahassee, Florida 32310, USA

⁶Department of Chemistry, Louisiana State University, Baton Rouge, Louisiana 70803, USA

(Received 23 July 2005; published 3 March 2006)

Strongly frustrated magnetism of the metallic pyrochlore oxide $\text{Pr}_2\text{Ir}_2\text{O}_7$ has been revealed by single crystal study. While Pr 4*f* moments have an antiferromagnetic RKKY interaction energy scale of $|T^*| = 20$ K mediated by Ir 5*d*-conduction electrons, no magnetic long-range order is found except for partial spin freezing at 120 mK. Instead, the Kondo effect, including a $\ln T$ dependence in the resistivity, emerges and leads to a partial screening of the moments below $|T^*|$. Our results indicate that the underscreened moments show spin-liquid behavior below a renormalized correlation scale of 1.7 K.

DOI: 10.1103/PhysRevLett.96.087204

PACS numbers: 75.20.Hr, 75.40.Cx, 75.50.Ee

Geometrically frustrated magnets have attracted great interest because of the possible emergence of novel magnetic phases at low temperatures resulting from the suppression of conventional order. Among them, the three-dimensional pyrochlore lattice of corner sharing tetrahedra has been studied extensively [1]. It is predicted theoretically that Heisenberg spins on a pyrochlore lattice with nearest-neighbor antiferromagnetic (AF) coupling form a spin-liquid state at $T = 0$ K [2]. However, only a few compounds are believed to display a spin-liquid phase, such as the insulator $\text{Tb}_2\text{Ti}_2\text{O}_7$ [3].

In metallic systems, the frustration inherent to the pyrochlore lattice might also lead to new types of electronic behavior. One remarkable possibility is the predominance of the Kondo effect, and concomitant heavy-fermion behavior, in nearly localized *d*- and *f*-electron systems where the Kondo temperature is generally too small to overcome magnetic order without the frustration. Prominent examples are the heavy-fermion behavior in LiV_2O_4 and $\text{Y}(\text{Sc})\text{Mn}_2$ with itinerant *d*-electron spins on a pyrochlore lattice [4,5].

Connecting the two exotic states of frustrated magnets, insulating spin-liquid and itinerant heavy fermions, there is another exciting yet unprecedented possibility of *metallic spin liquid* [6,7]. Ground states in *f*-electron based Kondo lattices are generally classified into Fermi liquid and magnetic regimes as the result of the competition between the Kondo effect and RKKY interactions. If the lattice has geometrical frustration and the transition temperature is depressed, the underscreened moments may stay disordered even in the magnetic regime, and form a metallic spin liquid on the *geometrically frustrated Kondo lattice*. (See the inset of Fig. 1.)

There has been a number of reports on *metallic* systems among the $\text{A}_2\text{B}_2\text{O}_7$ pyrochlore oxides possessing localized moments [1]. Yet, none is known to remain magnetically

disordered down to the lowest temperatures except for the newly developed pyrochlore iridates [8]. In particular, the AF correlated Pr 4*f* moments of $\text{Pr}_2\text{Ir}_2\text{O}_7$ remain paramagnetic down to at least 0.3 K in the metallic state due to the Ir 5*d*-conduction bands [8]. This places $\text{Pr}_2\text{Ir}_2\text{O}_7$ as a candidate for a geometrically frustrated Kondo lattice.

Here we report on strongly frustrated magnetism in single crystals of $\text{Pr}_2\text{Ir}_2\text{O}_7$. We find that the $\langle 111 \rangle$ Ising-like Pr^{3+} moments have an AF RKKY interaction energy scale $|T^*| = 20$ K. However, the dc magnetization down to 70 mK does not exhibit any trace of long-range order (LRO), except for an indication of partial freezing at 120 mK. Instead, the Kondo effect emerges below $|T^*|$ and leads to a partial screening of the 4*f* moments, re-

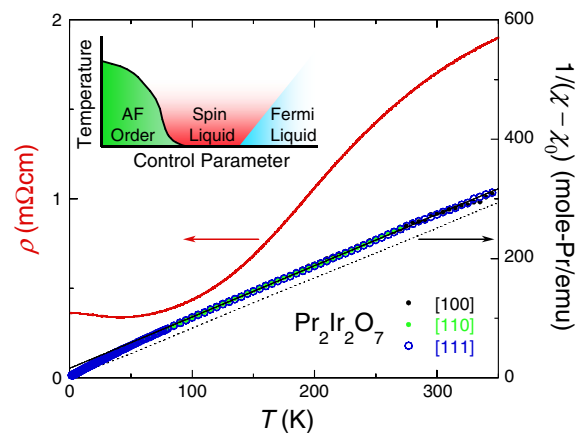


FIG. 1 (color online). Zero-field resistivity $\rho(T)$ (left axis), and the inverse of susceptibility $(\chi - \chi_0)^{-1}(T)$ (right axis) measured under a field of 100 mT along [100], [110], and [111]. The solid line represents a fit to the Curie-Weiss law, while the broken line indicates $(\chi_{\text{CEF}} - \chi_{\text{vv}})^{-1}$ based on the crystal electric field analysis. Inset: the schematic phase diagram for geometrically frustrated Kondo lattices.

normalizing the AF interaction to $|\theta_W| = 1.7$ K. Below $|\theta_W|$, the underscreened moments show spin-liquid behavior as indicated by the $\ln T$ dependence of the susceptibility and the $T^{1/2}$ dependence of the specific heat, as predicted for a frustrated Kondo lattice [6,7].

Single crystals of $\text{Pr}_2\text{Ir}_2\text{O}_7$ of 1 mm^3 in size were grown using a flux method for the first time at Kyoto [9]. A standard four-probe method was employed for resistivity measurements. Magnetotransport measurements were performed at the NHMFL dc field facility using a sample rotator. Specific heat C_p was measured by the thermal relaxation method down to 0.35 K. Magnetization measurements between 1.8 and 350 K were performed using a commercial SQUID magnetometer. Magnetization between 0.07 and 2.5 K and at fields up to 13 T was measured by the Faraday balance method using a dilution refrigerator at ISSP [10]. Single crystal four-axis x-ray diffraction analysis performed at LSU confirmed a well-ordered pyrochlore structure with $Fd\bar{3}m$ symmetry with $a = 10.3940(4) \text{ \AA}$ (300 K) and $10.3850(4) \text{ \AA}$ (105 K) [9]. Energy dispersive x-ray analysis measurements found no trace of impurities.

The metallic transport of $\text{Pr}_2\text{Ir}_2\text{O}_7$ is shown in Fig. 1. No anisotropy was found with respect to the current direction. The resistivity $\rho(T)$ steeply decreases on cooling and saturates at a large residual resistivity $\rho_0 \sim 360 \mu\Omega \text{ cm}$. On the other hand, a carrier density of $2.6 \times 10^{20} \text{ cm}^{-3}$ (1.8%/Pr), estimated from our preliminary Hall effect measurements at low T , yields a mobility of $\sim 70 \text{ cm}^2/\text{V sec}$ for a single carrier model. This confirms the high quality of our single crystals, and shows that the low carrier density is the origin of the large ρ_0 .

The crystal electric field (CEF) scheme of Pr^{3+} has been determined by inelastic neutron scattering measurements at 5 K [11]. Our analysis reveals the following two points: (i) nine multiplet levels of Pr^{3+} split into a ground-state doublet, three excited-singlets (162, 1218, 1392 K) and two excited doublets (580, 1044 K); and (ii) the Γ_3 ground-state doublet is magnetic with local $\langle 111 \rangle$ Ising anisotropy whose strength is ~ 160 K. Because of the large separation between CEF levels, the magnetism discussed below comes solely from the ground doublet.

The inverse susceptibility $(\chi - \chi_0)^{-1}(T)$ is shown in Fig. 1. No anisotropy is found under a field of 0.1 T applied along $[100]$, $[110]$, and $[111]$. $\chi_0 = 1.25 \times 10^{-3} \text{ emu/mole-Pr}$ is determined by a Curie-Weiss (CW) analysis above 100 K using the formula $\chi = \chi_0 + C/(T - T^*)$. This agrees with the sum of the Van Vleck term ($\chi_{\text{vv}} = 7.0 \times 10^{-4} \text{ emu/mole-Pr}$), as estimated from the above CEF scheme, and a Pauli paramagnetic term ($\chi_p \sim 5.0 \times 10^{-4} \text{ emu/mole-Ir}$) from the Ir $5d$ -conduction electrons, as in the metallic phase of $(\text{Y, Ca})_2\text{Ir}_2\text{O}_7$ [12]. The effective moment $g_J \sqrt{J_z(J_z + 1)} = 3.06 \mu_B$ for the ground doublet is lower than the Pr^{3+} multiplet value ($3.62 \mu_B$) due to the CEF. The AF Weiss temperature $T^* = -20.0$ K is most likely due to the RKKY interactions of the $4f$ moments for

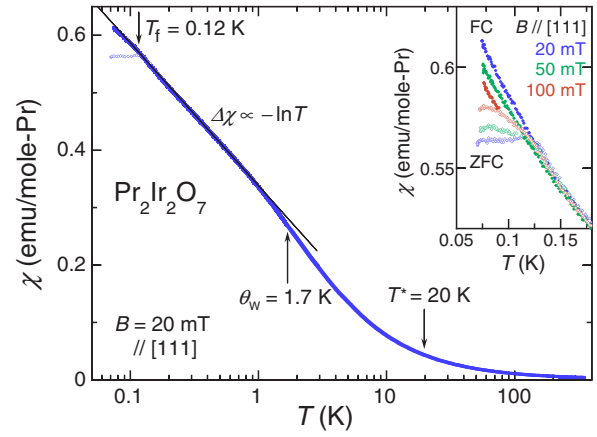


FIG. 2 (color online). dc susceptibility $\chi(T)$ as a function of $\ln T$ under a field of 20 mT along $[111]$. The $\ln T$ dependence is indicated by the solid line. Low T dependence under various fields is shown in the inset in a linear scale. Both field-cooled (FC) and zero-field-cooled (ZFC) data are shown.

the following three reasons. (i) CW analysis of the susceptibility $\chi_{\text{CEF}}(T)$ computed using the above CEF scheme indicates a negligibly small CEF contribution ($+0.77$ K) to T^* (Fig. 1). (ii) Single-ion Kondo coupling cannot be as large as 20 K. In fact, few Pr-based compounds show Kondo effect because of Hund coupling in the $\text{Pr}^{3+} 4f^2$ configuration which strongly reduces the Kondo temperature T_K [13]. Moreover, the low carrier concentration should also considerably decrease T_K [14]. (iii) The $4f$ moment superexchange and dipolar interactions in insulating pyrochlore magnets are normally of the scale of ~ 1 K. Actually, $T^* = +0.35$ K for $\text{Pr}_2\text{Sn}_2\text{O}_7$, an insulating analog of $\text{Pr}_2\text{Ir}_2\text{O}_7$ [15]. Thus, a several orders of magnitude stronger T^* indicates that it is due to the RKKY interaction.

Normally, one expects a Pr-based low carrier system like $\text{Pr}_2\text{Ir}_2\text{O}_7$ to be deep in a magnetic regime, and to exhibit magnetic LRO at the intersite interaction scale $|T^*|$, if the system has no magnetic frustration [16]. Remarkably, however, no anomalies due to a magnetic transition were detected in $\chi(T)$, except for freezing at $T_f = 120$ mK (Fig. 2). A large ratio $|T^*|/T_f = 170$ is a strong indication of frustrated magnetism in $\text{Pr}_2\text{Ir}_2\text{O}_7$. In addition, an anomalous $\ln T$ dependence of $\chi(T)$ was observed over a decade of T between T_f and 1.4 K. This diverging $\chi(T)$ as $T \rightarrow 0$ K, combined with an exact pyrochlore lattice symmetry, confirmed by single crystal x ray, excludes the possibility that the non-Kramers ground doublet is split into nonmagnetic singlets. Instead, this $\ln T$ dependence, distinct from the mean-field CW behavior, indicates that the $4f$ moments are strongly fluctuating even at $T \ll |T^*|$ owing to the magnetic frustration, forming a liquidlike short-range order. In addition, the zero-field-cooled (ZFC) $\chi(T)$ only levels off below T_f as set by a bifurcation of the field-cooled and ZFC curves (inset of Fig. 2). Normally for spin glasses, the ZFC curve is expected to show a steep decrease below T_f because most spins get

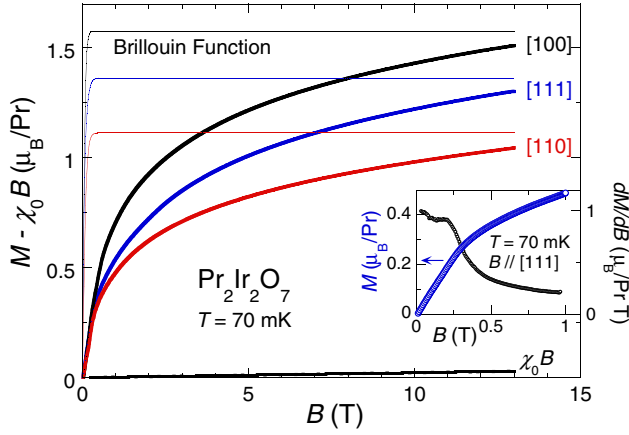


FIG. 3 (color online). Field dependence of the magnetization M (thick curves) and the Brillouin function of $\langle 111 \rangle$ Ising spins (thin curves) for fields along $[100]$, $[110]$, and $[111]$. Inset: low field M and its derivative dM/dB along $[111]$.

frozen at T_f . The observed T -independent behavior suggests that only a partial fraction of spins freezes, while the majority remain liquid.

The $\langle 111 \rangle$ Ising-like anisotropy of the $4f$ moments is confirmed by the field dependence of the magnetization $M(B)$ along $[100]$, $[110]$, and $[111]$ at 70 mK (Fig. 3). The $4f$ ground-state-doublet contribution (thick curves) is estimated by subtracting the sum of the Van Vleck and Pauli paramagnetic contributions, which is estimated from $\chi_0 B$ (Fig. 3). At 13 T, M tends to saturate and approaches a Brillouin function (thin curves) for noninteracting, local $\langle 111 \rangle$ Ising spins with $g_J J_z = 2.69$, consistent with the CEF analysis [11]. This slow saturation at the field scale, $B^* \equiv k_B |T^*| / (g_J \mu_B J_z) \sim 11$ T, confirms an AF coupling with an energy scale of $|T^*| = 20$ K. At low fields, M becomes isotropic (Fig. 3), as expected for $\langle 111 \rangle$ Ising spins on a pyrochlore lattice [17]. Below 0.3 T, M changes displaying a nearly constant derivative dM/dB (inset of Fig. 3). This departure from a Brillouin function also suggests liquidlike short-range correlations.

When such $\langle 111 \rangle$ Ising spins on a pyrochlore lattice interact only through a nearest-neighbor AF coupling J , mean-field theory predicts an “all-in and all-out” type of LRO to appear at $T \sim J$ [18]. This indicates that in $\text{Pr}_2\text{Ir}_2\text{O}_7$, effects beyond the mean-field theory of nearest-neighbor AF interaction, such as quantum fluctuations and longer-range couplings, are crucial to suppress the LRO down to $T \ll |T^*|$. Observed indications of such effects are (1) the Kondo coupling between the $4f$ moments and the $5d$ -conduction electrons, and (2) the RKKY long-range interactions between the $4f$ moments.

Although rare, the Kondo effect in Pr-based compounds [19,20] and low carrier systems [14] has been reported. The first evidence of Kondo effect in $\text{Pr}_2\text{Ir}_2\text{O}_7$ is the $\ln T$ dependence of the resistivity [Fig. 4(a)]. For such a dependence in a stoichiometric high-quality metal, two mechanisms can be considered: (i) CEF effect and (ii) Kondo

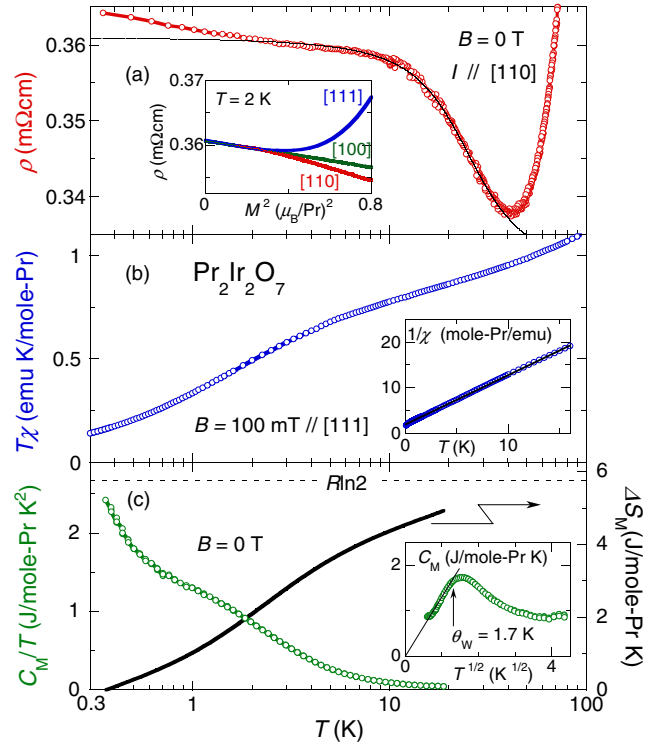


FIG. 4 (color online). (a) Low T resistivity $\rho(T)$ vs $\ln T$. Inset: transverse magnetoresistance vs the square of the magnetization M^2 along various axes. (b) Effective Curie constant $C(T) \equiv T\chi(T)$ vs $\ln T$. Inset: inverse susceptibility $\chi^{-1}(T)$. (c) Magnetic part of the specific heat divided by temperature C_M/T (left axis) and the entropy $\Delta S_M(T) \equiv S(T) - S(0.35 \text{ K})$ (right axis) as a function of $\ln T$. The horizontal broken line indicates $\Delta S_M(T) = R \ln 2$. Inset: C_M as a function of $T^{1/2}$.

effect. Since the gap to the first excited level is ~ 160 K, the $\ln T$ dependence below 50 K cannot be due to a CEF effect. Thus, the observed $\ln T$ dependence is likely due to the Kondo effect, and in fact, over a decade in T between 3 K and 35 K, $\rho(T)$ can be fit to the Hamann’s expression (solid line) with $T_K = 25$ K [21]. Interestingly, T_K is close to $|T^*|$, and suggests that it is not the single-ion screening, but the intersite screening that leads to the Kondo effect, as discussed for low carrier-density and AF correlated Kondo lattices [14,22]. In addition, the field dependence of the resistivity is consistent with the Kondo effect [13]; the negative magnetoresistance is proportional to M^2 for all axes under fields up to 2 T $< B^*$ [inset of Fig. 4(a)].

Second, the Kondo effect is also seen in the low T decrease of the effective Curie constant $C(T) \equiv T\chi(T)$; see Fig. 4(b). The rapid decrease in $C(T)$ below 10 K suggests that the moment size diminishes owing to Kondo screening. Correspondingly, $\chi^{-1}(T)$ follows the CW law over a decade in T from 1.5 to 16 K [solid line in the inset of Fig. 4(b)], yielding a slightly smaller effective moment $2.69\mu_B$, and a reduced Weiss temperature, $|\theta_W| = 1.7$ K, in comparison with the high T values ($3.06\mu_B$, 20 K). These results and the crossover to $\ln T$ dependence below $|\theta_W|$ indicate partial screening of $4f$ mo-

ments, which dramatically renormalizes the AF interaction energy scale and consequently leads to a correlated liquid of underscreened moments below $|\theta_W|$. The monotonic increase of $\rho(T)$ on cooling [Fig. 4(a)] indicates incoherent spin scattering in the spin-liquid state at $T < |\theta_W|$.

Further evidence for the Kondo effect and spin-liquid formation can be found in the T dependence of the magnetic part of the specific heat C_M . C_M is obtained by subtracting from C_P , (i) the lattice contribution estimated from $C_P(T)$ of the isostructural, $4f$ moment free $\text{Eu}_2\text{Ir}_2\text{O}_7$, and (ii) the $1/T^2$ Pr-nuclear quadrupole contribution estimated by a standard analysis of the field dependence. No evidence of LRO, but a rapid increase up to ~ 2.5 J/mole-Pr K^2 is seen in C_M/T below $|T^*|$, attributable to the Kondo screening [Fig. 4(c)]. Correspondingly, the entropy $\Delta S_M(T) \equiv S(T) - S(0.35 \text{ K})$ estimated by integrating C_M/T shows a gradual decrease from the $R \ln 2$ of the ground doublet below $|T^*| = 20$ K. Significantly, C_M forms a broad peak around $T \sim |\theta_W|$, and decreases on cooling with a $T^{1/2}$ dependence between 1.8 and 0.4 K [inset of Fig. 4(c)]. This peak indicates the formation of a correlated spin-liquid below $|\theta_W|$. S_M also follows the $T^{1/2}$ dependence at low T s, indicating the presence of much more highly degenerate magnetic states than in a Fermi liquid with a T -linear entropy. This also represents additional evidence for magnetic frustration.

The experiments reported here reveal the following remarkable properties: (1) a large ratio $|T^*|/T_f = 170$, (2) Kondo effect below $|T^*|$, (3) $\ln T$ dependence of $\chi(T)$ below $|\theta_W|$, (4) peak formation of C_M at $T \sim |\theta_W|$ with a $T^{1/2}$ dependence below $|\theta_W|$, and (5) a linear increase of the low- T $M(H)$ below $B_c = 0.3$ T. Observations (1) and (2) indicate that $\text{Pr}_2\text{Ir}_2\text{O}_7$ is a strongly frustrated Kondo lattice, most likely ascribable to the geometrical frustration inherent to the pyrochlore structure. Moreover, observations (3)–(5) indicate spin-liquid behavior at $T \leq |\theta_W|$ and $B \leq B_c$. The boundaries $|\theta_W|$ and B_c have energy scales of the same order of magnitude, as evident from the relation $k_B|\theta_W|/(g_J\mu_B J_z) = 0.9$ T.

Notably, observations (3) and (4), especially the T dependence of χ and C_M , agree well with the spin-liquid behavior predicted by dynamical mean-field theory for a frustrated Kondo lattice [6,7]. Near a quantum critical point separating spin-liquid and Fermi liquid (see the inset of Fig. 1), the ground state is expected to be so sensitive to disorder that even undetectable defects may cause spin freezing [7]. The observed low T cutoff of the asymptotic forms of $\chi(T) \propto \ln T$ and $C_M \propto T^{1/2}$ may come from a tendency towards spin freezing of the decoupled spins caused by disorder [7]. To confirm this, μSR measurements are now in progress.

To summarize, our single crystal study has revealed that $\text{Pr}_2\text{Ir}_2\text{O}_7$ is a pyrochlore Kondo lattice with $\langle 111 \rangle$ Ising-like $4f$ moments. The following four-stage process is observed: (1) $T > |T^*|$, Pr $4f$ moments are decoupled from Ir $5d$ -conduction electrons; (2) $|T^*| > T > |\theta_W|$, the

Kondo effect leads to the screening of the $4f$ moments; (3) $|\theta_W| > T > T_f$, underscreened moments form a spin liquid; and (4) $T_f > T$, the moments partially freeze. The magnetic LRO expected at the RKKY coupling scale is suppressed due to geometrical frustration, but instead the Kondo effect is stabilized to partially screen the $4f$ moments, and leads to the “metallic spin-liquid” behavior. Further investigation is necessary to clarify the origin of the geometrical frustration in the pyrochlore magnet.

We thank C. Broholm, V. Dobrosavljević, D.E. MacLaughlin, H. Tsunetsugu, R. Moessner, K. Ishida, and T. Kamata for discussions. This work is supported in part by Grants in Aids for Scientific Research from JSPS and for the 21st Century COE “Center for Diversity and Universality in Physics” from MEXT of Japan, and by the Nippon Sheet Glass Foundation. The NHMFL is supported by NSF DMR-0084173, and J. Y. C. by the NSF DMR-0237664 and the Alfred P. Sloan Foundation.

-
- [1] M. A. Subramanian, G. Aravamudan, and G. V. Subba Rao, *Prog. Solid State Chem.* **15**, 55 (1983).
 - [2] J. Villain, *Z. Phys. B* **33**, 31 (1979); J. N. Reimers, A. J. Berlinsky, and A.-C. Shi, *Phys. Rev. B* **43**, 865 (1991); R. Moessner and J. T. Chalker, *Phys. Rev. Lett.* **80**, 2929 (1998); B. Canals and C. Lacroix, *Phys. Rev. Lett.* **80**, 2933 (1998).
 - [3] J. S. Gardner *et al.*, *Phys. Rev. Lett.* **82**, 1012 (1999).
 - [4] S. Kondo *et al.*, *Phys. Rev. Lett.* **78**, 3729 (1997).
 - [5] M. Shiga, K. Fujisawa, and H. Wada, *J. Phys. Soc. Jpn.* **62**, 1329 (1993).
 - [6] S. Burdin, D. R. Grempel, and A. Georges, *Phys. Rev. B* **66**, 045111 (2002).
 - [7] D. Tanasković, V. Dobrosavljević, and E. Miranda, *Phys. Rev. Lett.* **95**, 167204 (2005).
 - [8] D. Yanagishima and Y. Maeno, *J. Phys. Soc. Jpn.* **70**, 2880 (2001).
 - [9] J. N. Millican *et al.* (to be published).
 - [10] T. Sakakibara, H. Mitamura, T. Tayama, and H. Amitsuka, *Jpn. J. Appl. Phys.* **33**, 5067 (1994).
 - [11] Y. Machida *et al.*, *J. Phys. Chem. Solids* **66**, 1435 (2005).
 - [12] H. Fukazawa and Y. Maeno, *J. Phys. Soc. Jpn.* **71**, 2578 (2002).
 - [13] A. C. Hewson, *The Kondo Problem of Heavy Fermions* (Cambridge University Press, Cambridge, England, 1993).
 - [14] T. Suzuki, *Jpn. J. Appl. Phys. Ser. 8*, 268 (1993).
 - [15] K. Matsuhira *et al.*, *J. Phys. Soc. Jpn.* **71**, 1576 (2002).
 - [16] W. E. Wallace, *Rare Earth Intermetallics* (Academic, New York, 1973).
 - [17] R. Siddharthan *et al.*, *Phys. Rev. Lett.* **83**, 1854 (1999).
 - [18] S. T. Bramwell and M. J. Harris, *J. Phys. Condens. Matter* **10**, L215 (1998).
 - [19] P. Lethuillier and P. Haen, *Phys. Rev. Lett.* **35**, 1391 (1975).
 - [20] H. Sato *et al.*, *Phys. Rev. B* **62**, 15 125 (2000); K. Ishida *et al.*, *Phys. Rev. B* **71**, 024424 (2005).
 - [21] D. R. Hamann, *Phys. Rev.* **158**, 570 (1967).
 - [22] S. Nakatsuji *et al.*, *Phys. Rev. Lett.* **89**, 106402 (2002).

Spin Disorder on a Triangular Lattice

Satoru Nakatsuji,^{1*} Yusuke Nambu,¹ Hiroshi Tonomura,¹
Osamu Sakai,¹ Seth Jonas,³ Collin Broholm,^{3,4}
Hirokazu Tsunetsugu,² Yiming Qiu,^{4,5} Yoshiteru Maeno^{1,6}

As liquids crystallize into solids on cooling, spins in magnets generally form periodic order. However, three decades ago, it was theoretically proposed that spins on a triangular lattice form a liquidlike disordered state at low temperatures. Whether or not a spin liquid is stabilized by geometrical frustration has remained an active point of inquiry ever since. Our thermodynamic and neutron measurements on NiGa_2S_4 , a rare example of a two-dimensional triangular lattice antiferromagnet, demonstrate that geometrical frustration stabilizes a low-temperature spin-disordered state with coherence beyond the two-spin correlation length. Spin liquid formation may be an origin of such behavior.

Electronic magnetic moments (spins) in magnets generally develop periodic order at low temperatures. When such order is suppressed, however, qualitatively new quantum phases can emerge. For example, quantum spin liquids appear in quasi-one-dimensional spin chains when fluctuations enhanced by low dimensionality destabilize static correlations (1). In higher dimensions, magnetic order may also be suppressed because of the geometry of the crystal lattice. Such an effect occurs, for example, in an antiferromagnet with a structure formed by arrays of triangles. Antiferromagnetically interacting spins on the vertices of triangles cannot simultaneously satisfy all pairwise interactions and may remain disordered well below the conventional ordering scale set by the Weiss temperature, θ_w (2). Thus, “geometrical frustration” promotes high degeneracy among competing low-temperature phases, enhances quantum fluctuations, and may lead to unconventional quantum phenomena.

In two dimensions, the simplest form of a geometrically frustrated lattice is a triangular lattice with a single magnetic atom per unit cell. This is the system for which a quantum spin-disordered state in more than one dimension was first proposed more than three decades ago (3). Since then, extensive theoretical and experimental research has been carried out in pursuit of novel ground states without magnetic order in

two dimensions. Although it is now believed that triangular lattice antiferromagnets with nearest-neighbor coupling exhibit 120° spin order (4–6), recent theories suggest that interactions beyond nearest-neighbor exchange, such as longer range and multiple-spin exchange interactions, may lead to a quantum spin-disordered ground state (7, 8). Experimentally, however, only a few candidates for spin-disordered states in two dimensions have been reported, in an organic material with a distorted triangular lattice (9), in Kagomé-related antiferromagnets (10, 11), and in a low-density solid ^3He film adsorbed on a graphite surface (12). So far unanswered is the question of whether an insulating bulk solid with an exact triangular lattice

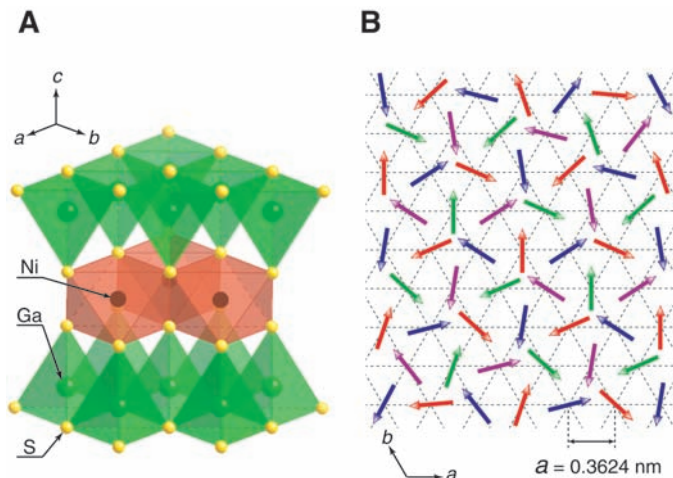
of well-defined localized moments can exhibit a novel ground state without magnetic order.

We demonstrate that high-quality samples of NiGa_2S_4 , a bulk-insulating antiferromagnet on an exact triangular lattice, exhibit a spin-disordered state in two dimensions. Despite strong antiferromagnetic (AF) interactions, no magnetic long-range order was observed down to 0.35 K, where we instead found nanoscale quasi-static correlation. The spin-disordered state appeared on cooling through highly degenerate states with an entropy plateau and exhibited gapless, linearly dispersive modes, suggesting coherence beyond the two-spin correlation length. The gapless excitations were insensitive to a magnetic field but sensitive to impurities. These observations indicate the absence of canonical spin glass freezing in the bulk, raising the possibility of a spin liquid state with slow dynamics.

NiGa_2S_4 is a layered chalcogenide magnetic insulator with a stacked triangular lattice of Ni spins (13) (Fig. 1A). The structure is highly two-dimensional (2D) and the central NiS_2 layer is isostructural with the CoO_2 layer in superconducting $\text{Na}_x\text{CoO}_2 \cdot y\text{H}_2\text{O}$ (14). Magnetism is associated with Ni^{2+} with the electronic configuration $t_{2g}^6 e_g^2$ and spin $S = 1$. The unit cell contains a single Ni^{2+} atom, so the intra- and inter-plane Ni separations are simply given by the lattice parameters $a = 0.3624$ nm and $c = 1.1999$ nm.

In Fig. 2A, the temperature dependence of the magnetic susceptibility, $\chi(T) \equiv M(T)/B$, and its inverse, $\chi^{-1}(T)$, where T is the temperature, are presented. The applied field B

Fig. 1. Crystal and spin structures of NiGa_2S_4 . (A) The slab structure of NiGa_2S_4 consists of a central NiS_2 layer of edge-sharing NiS_6 octahedra (red) and top and bottom sheets of GaS_4 tetrahedra (green). The slabs are stacked along the c axis and separated from each other by a van der Waals gap. Polycrystalline samples of NiGa_2S_4 were synthesized by heating the mixture of elements Ni, Ga, and S in evacuated silica ampoules at 900°C . Our powder x-ray measurements at room temperature and neutron diffraction measurements in the temperature range 1.5 K to 300 K confirmed that NiGa_2S_4 retains the trigonal crystal structure down to 1.5 K with $P\bar{3}m1$ symmetry. The refinements are consistent with the room-temperature structure (13). (B) The short-range correlated spin structure on the triangular Ni lattice, including the incommensurability observed by magnetic neutron diffraction. It approximates four independent 120° structures on the colored sublattices with lattice parameters $2a$. The in-plane correlation length is $2.5(3)$ nm, and the correlation time exceeds 0.3 ns. There are weak ferromagnetic correlations between nearest-neighbor planes.



¹Department of Physics, ²Yukawa Institute for Theoretical Physics, Kyoto University, Kyoto 606-8502, Japan. ³Department of Physics and Astronomy, Johns Hopkins University, Baltimore, MD 21218, USA. ⁴NIST Center for Neutron Research, National Institute of Standards and Technology (NIST), Gaithersburg, MD 20899, USA. ⁵Department of Materials Science and Engineering, University of Maryland, College Park, MD 20742, USA. ⁶International Innovation Center, Kyoto University, Kyoto 606-8501, Japan.

*To whom correspondence should be addressed. E-mail: nakatsuji@scphys.kyoto-u.ac.jp

was 7 T, a field at which the magnetization M remains proportional to B . No difference was found between field-cooled and zero field-cooled data. Susceptibility above 150 K followed the Curie-Weiss law: $\chi^{-1}(T) = (T - \theta_w)/C$, and the Curie constant C corresponds to an effective moment of 2.81(3) Bohr magnetons (μ_B), consistent with spin-1 ($S = 1$) Ni^{2+} . The Weiss temperature, $\theta_w = -80(2)$ K, indicates strong AF interactions. However, in a field of 7 T, no sharp magnetic anomaly or field hysteresis was observed down to 1.8 K. Instead, the susceptibility smoothly increased on cooling and passed through a shallow and broad maximum at $T \sim 10$ K before approaching a finite low- T limit. These data exclude the possibility of a conventional spin-gap system in which the susceptibility vanishes exponentially at low temperatures.

Specific heat data, $C_p(T)$, also showed no evidence of a phase transition for fields between 0 T and 7 T and temperatures from 175 K down to 0.35 K (Fig. 2B, inset). These data indicate a disordered low-temperature state without conventional AF order. We probed the density of states for spin excitations through the magnetic specific heat $C_M(T)$ after subtraction of the lattice contribution (15). $C_M(T)$ (Fig. 2B) exhibited an unusual double-peak structure. One peak was broad and centered around $T = |\theta_w|$, below which the susceptibility was suppressed compared to the one expected from the high-temperature Curie-Weiss law (Fig. 2A). The lower temperature peak featured a prominent rounded maximum at $T_{\text{peak}} \sim 10$ K, where $\chi(T)$ also showed a broad maximum. The entropy S_M , obtained through integration of C_M/T (Fig. 2B), correspondingly had a plateau at $S_M \approx \frac{1}{3} R \ln 3$ before high- T saturation at $S_M \approx R \ln 3$, where R is the gas constant. This indicates high degeneracy of low-energy states because of magnetic frustration and is similar to predictions for the spin-1/2 antiferromagnet on the Kagomé lattice of corner-sharing triangles (16).

The specific heat exhibited power-law behavior at low temperatures (Fig. 3). The data between 0.35 and 4.0 K are well fitted by a power law $C_M = AT^\alpha$, where A is a constant and α is 2.001(5) (Fig. 3A). Quadratic temperature dependence through one decade indicates the presence of gapless and linearly dispersive modes in two dimensions. A gapless spectrum is furthermore consistent with a finite value of the susceptibility in the low- T limit. If the low- T specific heat peak were associated with AF ordering of individual $S = 1$ spins, it would be suppressed under a magnetic field of $k_B T_{\text{peak}}/g\mu_B \sim 7$ T, where k_B is the Boltzmann constant and g is the g factor. Instead, the specific heat was unaffected by fields up to 7 T, indicating that the low- T peak reflects short-range correlations among composite degrees of freedom that do not directly couple to a uniform field (17). It follows that the linearly dispersive

excitations implied by $C_M \propto T^2$ are collective modes of moment-free spin clusters. Likewise, the specific heat peak at high $T \sim |\theta_w|$ and the concomitant suppression of the susceptibility compared to the one expected from high-temperature Curie-Weiss law are attributable to the formation of incoherent moment-free spin clusters. Similar thermodynamic properties have been reported for the Kagomé-related antiferromagnets, $\text{SrCr}_9\text{Ga}_{12-9p}\text{O}_{19}$ (10, 17), and for deuterium jarosite (11).

Although no susceptibility anomaly was observed at 7 T, weak field dependence and hysteresis was observed at low fields for temperatures below a freezing temperature $T_f = 8.5$ K (Fig. 3B). Previous work indicates that minute levels of quenched disorder can induce spin freezing in geometrically frustrated magnets (2). However, the bifurcation of $\chi(T)$ in NiGa_2S_4 is distinct from previous observations in frustrated magnets in that it involves only a small component of the whole susceptibility

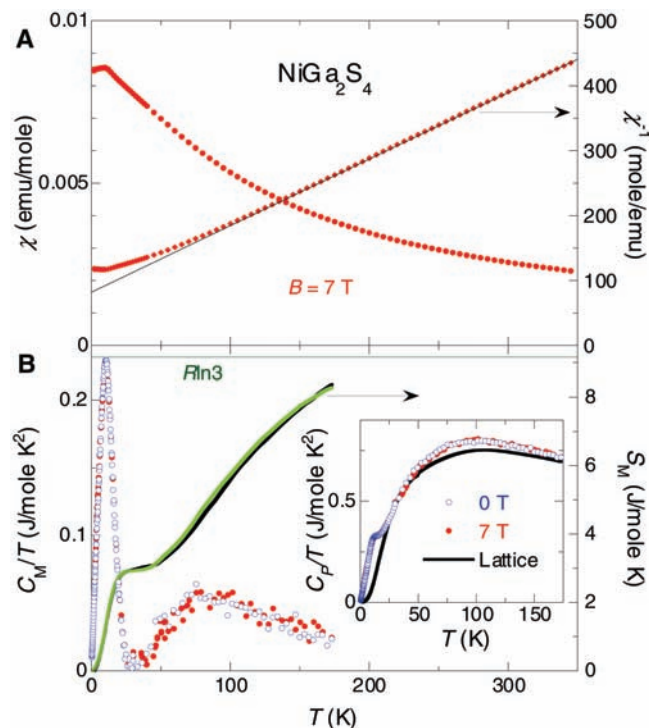


Fig. 2. Temperature dependence of the susceptibility and specific heat of polycrystalline NiGa_2S_4 . (A) The susceptibility χ (circles, left axis) and inverse susceptibility χ^{-1} (diamonds, right axis), measured at 7 T with a superconducting quantum interference device (SQUID) magnetometer (Quantum Design, model MPMS-XL). The solid line is the Curie-Weiss fit, emu, electromagnetic unit. (B) The magnetic part of the specific heat divided by temperature C_M/T (left axis) at zero field (blue open circles) and at 7 T (red solid circles) and the entropy S_M (right axis) at 0 T (green line) and at 7 T (black line). The horizontal line indicates $S_M = R \ln 3$. Inset: C_p/T for NiGa_2S_4 at 0 T (blue open circles) and 7 T (red solid circles) and its lattice part C_L/T [black solid line (15)].

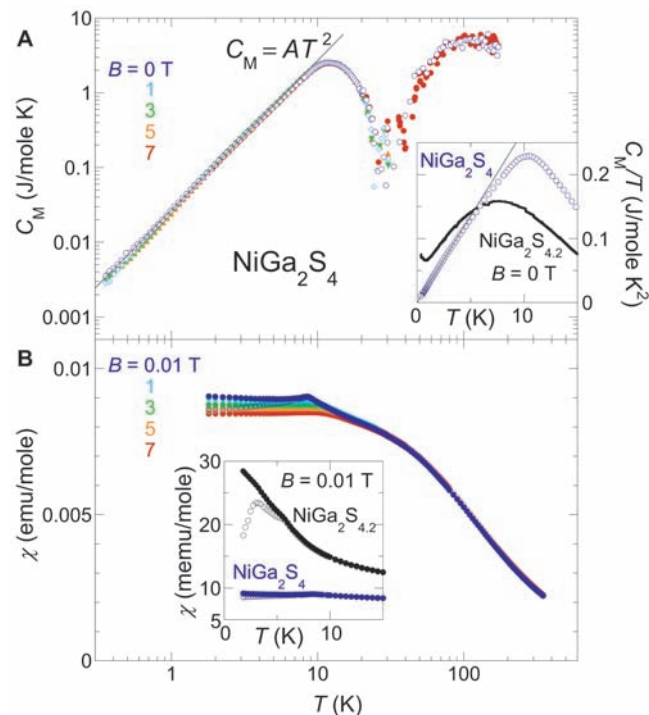


Fig. 3. Magnetic field dependence of the specific heat and susceptibility of NiGa_2S_4 . (A) The magnetic part of the specific heat C_M under different fields versus temperature in full logarithmic scale. Inset: C_M/T versus temperature under zero field for NiGa_2S_4 and the sample with nominal doping of excess 5% sulfur, $\text{NiGa}_2\text{S}_{4.2}$. The solid lines show the T^2 dependence of C_M . (B) The susceptibility χ under different fields. Inset: The low-temperature part of χ for NiGa_2S_4 and $\text{NiGa}_2\text{S}_{4.2}$ at 0.01 T. Both field-cooled (solid circles) and zero field-cooled (open circles) data are shown.

(~5%). The following observations indicate that it may in fact be a surface effect. First, intentional impurity doping by 5% excess sulfur leads to a substantial enhancement of freezing behavior (18). A large value of $C_M(T)/T$ (~70 mJ/mol K²) was induced for $T \rightarrow 0$ and hysteresis in $\chi(T)$ was strongly enhanced (Fig. 3, inset). Second, when a field around the critical value $B_c \sim 7$ T was applied, the hysteretic part of the susceptibility completely disappeared, whereas the specific heat, $C_M(T)$, showed only negligible field dependence in the same B - T range. Because magnetism is extremely sensitive to imperfection, the different field effects of the two thermodynamic quantities, together with $C_M(T)/T \rightarrow 0.0(1)$ mJ/mol K² as $T \rightarrow 0$ K, indicate that the hysteretic part of the susceptibility is associated with a very small density of impurities. In addition, the value of B_c implies that impurity spins are individual $S = 1$ objects, as this value agrees with the magnetic field where $S = 1$ impurity spins become polarized, $B_c \sim k_B T_f / g \mu_B$. Third, the density of spins involved in freezing can be estimated from the difference between $\chi(T)$ for $B = 0$ T and 7 T, which follows a Curie-Weiss law with $\theta_w = 9$ K and an effective moment corresponding to 300 parts per million (ppm) of the Ni sites. This concentration matches that of surface spins in the $\sim 10 \mu\text{m}^3$ grains of our sample. Finally, this small density of impurities is consistent with diffraction measurements. No trace of disorder or impurities was found by x-ray or neutron powder diffraction, and Rietveld refinement of neutron powder diffraction data is consistent with the nominal stoichiometry.

To investigate low-energy spin correlations, we performed a magnetic neutron scattering experiment (19). Figure 4 shows the difference in elastic powder neutron scattering between $T = 1.5$ K and 15 K. The signal was resolution-limited in energy [$\delta E = 0.10$ meV, where δE is full width at half maximum (FWHM) energy resolution], which allows us to conclude that the

correlations persist on a time scale that exceeds 0.3 ns. The absence of a difference signal in the $Q \rightarrow 0$ limit, where Q is the scattering wave vector, indicates a correlated state built from moment-free spin clusters. Classical spins on a triangular lattice with nearest-neighbor AF interactions should develop correlations of the 120° variety with wave vector $\mathbf{q} = (\frac{1}{3}, \frac{1}{3}, 0)$. NiGa₂S₄ exhibited a peak at $Q_M = 0.57(1) \text{ \AA}^{-1} \approx 2\pi/3a = 0.5779 \text{ \AA}^{-1}$, which is the length of $\mathbf{q} = (\frac{1}{6}, \frac{1}{6}, 0)$. To understand this result, we compared the data to the spherical average of magnetic scattering from a quasi-2D magnet:

$$\frac{\partial \sigma}{\partial \Omega} = r_0^2 \frac{g}{2} F(Q)^2 N \sum_{\tau} (|m_{\mathbf{q}}|^2 - |\hat{\mathbf{Q}} \cdot \mathbf{m}_{\mathbf{q}}|^2) \times [1 + 2\alpha \cos(\mathbf{Q} \cdot \mathbf{c})] \frac{A^* \kappa^2 / \pi}{[(\mathbf{Q} - \tau \pm \mathbf{q})^2 + \kappa^2]^2} \quad (1)$$

Here σ is the scattering cross section, Ω is the solid angle of detection, $r_0 = 5.4 \times 10^{-15}$ m, F is the magnetic form factor for Ni²⁺, N is the number of magnetic ions, A^* is the area of the Brillouin zone, and the summation is over 2D reciprocal lattice vectors τ . The spin expectation value on site, r , averaged over a time interval that exceeds 0.3 ns, is given by $\langle S_r \rangle = \mathbf{m}_{\mathbf{q}} e^{i\mathbf{q} \cdot \mathbf{r}} + \mathbf{m}_{\mathbf{q}}^* e^{-i\mathbf{q} \cdot \mathbf{r}}$, where $\mathbf{m}_{\mathbf{q}}$ is a complex vector. In Eq. 1, κ is the inverse 2D correlation length and $\alpha = \langle \mathbf{S}_0 \cdot \mathbf{S}_{\pm \mathbf{c}} \rangle \langle \mathbf{S}_0 \cdot \mathbf{S}_0 \rangle^{-1}$ represents nearest-neighbor inter-plane correlations. When \mathbf{q} was not $(\frac{1}{3}, \frac{1}{3}, 0)$, there were three symmetry-related wave vector domains. The line in Fig. 4 corresponds to $\mathbf{q} = (\eta, \eta, 0)$ with $\eta = 0.158(1)$ and $\mathbf{m}_{\mathbf{q}} = \hat{x} m_{qx} + i\hat{y} m_{qy} + \hat{z} m_{qz}$, where $m_{qx} = 0.31(3)$, $m_{qy} = 0.43(4)$, and $m_{qz} = 0.0(1)$. Here $\hat{z} \parallel \mathbf{c}$ and \hat{x}, \hat{y} are parallel and perpendicular to \mathbf{q} , respectively. The corresponding time- and site-averaged spin is $|\langle S \rangle| = \sqrt{(\frac{1}{N} \sum_r \langle S_r^2 \rangle)} = \sqrt{2|\mathbf{m}_{\mathbf{q}}|} = 0.75(8)$. This value is notably reduced from $S = 1$ for Ni²⁺ because of quantum fluctuations

enhanced by frustration and low dimensionality. It is also important that the in-plane correlation length, $\xi = \kappa^{-1} = 2.5(3)$ nm, corresponds to 6.9(8) triangular lattice spacings and $\sim 2.5 \times 10^{-4}$ times the powder sample grain size. Ferromagnetic inter-plane correlations were limited to nearest neighbors as indicated by $\alpha = 0.25(5)$.

The incommensurate short-range order inferred from the diffraction data (Fig. 1B) has various possible explanations. If third-neighbor AF interactions, J_3 , dominate, magnetic orders with $\mathbf{q} = (\frac{1}{6}, \frac{1}{6}, 0)$ and/or $(\frac{1}{3}, \frac{1}{3}, 0)$ will be degenerate at the mean field level. Nearest neighbor couplings, J_1 , lift the degeneracy. When J_1 is ferromagnetic, a $(\frac{1}{6}, \frac{1}{6}, 0)$ order is favored, but the wave vector will be shifted to an incommensurate value $(\eta, \eta, 0)$, as in our diffraction data. From the experimental value of $\eta = 0.158(1)$, mean field theory yields $J_1/J_3 = -0.2(1)$. Indeed, because the nearest-neighbor Ni-S-Ni bond angle was near 90°, J_1 should be small and potentially ferromagnetic. Alternatively, proximity of the NiS₂ layer to a metal-insulator transition may produce multiple-spin exchange that stabilizes a larger unit cell.

Although the spin correlation length, $\xi = 2.5(3)$ nm, is rather short, specific heat data indicate a much longer coherence length for low-energy excitations. When coherent propagation of excitations is limited up to a length scale L_0 at $T = 0$, the specific heat deviates from the low- T asymptotic form as $C_M/R = -(\sqrt{3}\pi/2)(a/L_0)^2 + [3\sqrt{3}\zeta(3)/2\pi](ak_B T/\hbar D)^2$ at $\hbar D/(L_0 k_B) \ll T \ll \theta_w$, where D is the spin stiffness constant (20). Least-squares fitting of this expression to the specific heat data in Fig. 3 yields a lower bound, $L_0 > 200$ nm. Clearly, this is far greater than the two-spin correlation length, $\xi = 2.5(3)$ nm, determined by neutron diffraction, and it indicates that coherent low-energy modes are a bulk effect in NiGa₂S₄.

These experimental results demonstrate that NiGa₂S₄ has unique low-temperature properties: (i) absence of conventional magnetic order, which is replaced by incommensurate short-range order with nanoscale correlation; (ii) absence of canonical bulk spin glass freezing; (iii) gapless coherent excitations in two dimensions that are insensitive to field but sensitive to impurities; and (iv) highly degenerate low-energy states as indicated by an entropy plateau. These observations place strong constraints on possible ground states. One likely candidate is a spin liquid with no conventional magnetic long-range order as characterized by resolution-limited Bragg peaks, no static spin freezing, and an absence of spin dimerization (i.e., valence bond solid order) that would induce a finite spin gap. Observations (i), (ii), and (iii) are consistent with these criteria. Moreover, observations (iii) and (iv) are consistent with the type of spin liquid that is expected to result from quantum effects in a highly degenerate manifold induced by mag-

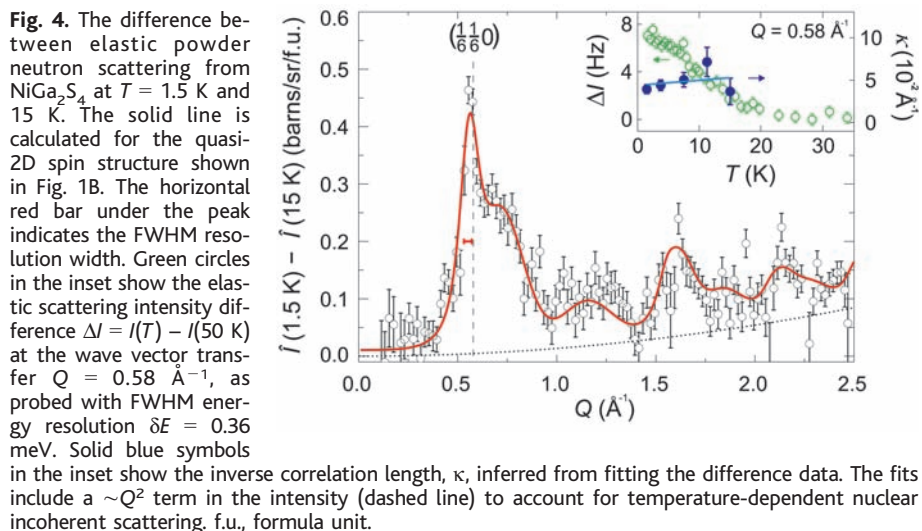


Fig. 4. The difference between elastic powder neutron scattering from NiGa₂S₄ at $T = 1.5$ K and 15 K. The solid line is calculated for the quasi-2D spin structure shown in Fig. 1B. The horizontal red bar under the peak indicates the FWHM resolution width. Green circles in the inset show the elastic scattering intensity difference $\Delta I = I(T) - I(50 \text{ K})$ at the wave vector transfer $Q = 0.58 \text{ \AA}^{-1}$, as probed with FWHM energy resolution $\delta E = 0.36$ meV. Solid blue symbols in the inset show the inverse correlation length, κ , inferred from fitting the difference data. The fits include a $\sim Q^2$ term in the intensity (dashed line) to account for temperature-dependent nuclear incoherent scattering. f.u., formula unit.

netic frustration. For example, recent theoretical work on the single-band Hubbard model on the triangular lattice suggests that a gapless spin liquid phase is realized at intermediate correlations (8). It is also predicted that the spin liquid phase has both spin-zero and non-zero low energy excitations (21) and incommensurate short-range correlation (22), which may be related to these observations.

Another possibility is a delicate form of long-range order that is dynamically inaccessible in real materials because of impurity pinning close to quantum criticality. Other possible ground states include a Kosterlitz-Thouless (KT) phase driven by two-valued vortices with the transition around T_{peak} (23) and a long-range order without long-range spin correlations such as in a spin nematic (24). The KT phase discussed here is not a conventional one but has a finite spin-correlation length, consistent with our observations. The neutron scattering data show that a large part of the magnetic spectral weight is associated with a long time scale that exceeds 0.3 ns. Experiments characterizing slow spin dynamics are in progress to distinguish between these exotic potential ground states in NiGa_2S_4 .

Like the spin-1/2 chain in one dimension (1), the triangular lattice antiferromagnet, which is the only geometrically frustrated 2D Bravais lattice, plays a central role in the search for cooperative phenomena in two dimensions. With AF nearest-neighbor interactions, Ising spins have residual entropy (25), and classical Heisenberg spins have a KT-type transition and noncolinear Néel order at $T = 0$ (23). In the extreme quantum spin-1/2 case, a superposition of singlet coverings constituting a resonating valence bond state was first introduced to describe the ground state of the triangular lattice antiferromagnet (3). Although it is now believed that a nearest-neighbor Heisenberg spin-1/2 model has 120° order at $T = 0$ (4–6), one may expect various exotic phases in real materials, driven by other effects such as longer range interactions, multiple-spin exchange, and structural dimerization. Consequentially, there have been intensive experimental searches for an ideal quasi-2D triangular lattice antiferromagnet with a small spin quantum number ($S \leq 1$) (26). Several spin-1/2 triangular lattices have been reported to show nonordered gapless phases, but all the materials so far have either a distorted structure (9, 27) or are only available in minute quantities, which limits accessibility for many experimental techniques (12).

To our knowledge, NiGa_2S_4 is the first low spin ($S \leq 1$), quasi-2D bulk magnet on an exact regular triangular lattice. Our measurements on NiGa_2S_4 demonstrate that geometrical frustration can be used to stabilize a spin-disordered state at low temperatures. A strongly fluctuating spin state has been discovered in a triangular lattice plane that is isostructural to the superconducting CoO_2 layer of $\text{Na}_x\text{CoO}_2 \cdot y\text{H}_2\text{O}$

(14) and is stoichiometric with NiS_2 , a metal-insulator transition system (28). It may thus be possible to drive NiGa_2S_4 into a conducting state in which the magnetic fluctuations have a qualitative effect on carrier correlations.

References and Notes

1. I. Affleck, *J. Phys. Condens. Matter* **1**, 3047 (1989).
2. A. P. Ramirez, in *Handbook of Magnetic Materials*, K. J. H. Buschow, Ed. (Elsevier Science, Amsterdam, 2001), vol. 13, pp. 423–520.
3. P. W. Anderson, *Mater. Res. Bull.* **8**, 153 (1973).
4. D. A. Huse, V. Elser, *Phys. Rev. Lett.* **60**, 2531 (1988).
5. B. Bernu, C. Lhuillier, L. Pierre, *Phys. Rev. Lett.* **69**, 2590 (1992).
6. L. Capriotti, A. E. Trumper, S. Sorella, *Phys. Rev. Lett.* **82**, 3899 (1999).
7. G. Misguich, C. Lhuillier, in *Frustrated Spin Systems*, H. T. Diep, Ed. (World-Scientific, Singapore, 2004), pp. 229–306.
8. H. Morita, S. Watanabe, M. Imada, *J. Phys. Soc. Jpn.* **71**, 2109 (2002).
9. Y. Shimizu, K. Miyagawa, K. Kanoda, M. Maesato, G. Saito, *Phys. Rev. Lett.* **91**, 107001 (2003).
10. A. P. Ramirez, G. P. Espinosa, A. S. Cooper, *Phys. Rev. Lett.* **64**, 2070 (1990).
11. A. S. Wills, A. Harrison, S. A. M. Mentink, T. E. Mason, Z. Tun, *Europhys. Lett.* **42**, 325 (1998).
12. K. Ishida, M. Morishita, K. Yawata, H. Fukuyama, *Phys. Rev. Lett.* **79**, 3451 (1997).
13. H. D. Lutz, W. Buchmeier, H. Siwert, *Z. Anorg. Allg. Chem.* **533**, 118 (1986).
14. K. Takada *et al.*, *Nature* **422**, 53 (2003).
15. The specific heat, C_p , was measured by a thermal relaxation method down to 0.35 K under fields up to 7 T. In order to estimate the lattice part of the specific heat, C_l , we measured C_p for the isostructural nonmagnetic analog ZnIn_2S_4 and obtained the thermal variation of the Debye temperature $\theta_D(T)$ using the Debye equation (29). $\theta_D(T)$ of NiGa_2S_4 was then estimated by applying a scale factor according to $\theta_D \propto M_0^{-1/2} V_0^{-1/3}$, where M_0 and V_0 are molar mass and volume, respectively. Finally, C_l was estimated by converting the scaled $\theta_D(T)$ data into specific heat. The magnetic part, C_M , was estimated as the difference between the total specific heat, C_p , and the lattice estimation C_l .
16. P. Sindzingre *et al.*, *Phys. Rev. Lett.* **84**, 2953 (2000).
17. A. P. Ramirez, B. Hessen, M. Winklemann, *Phys. Rev. Lett.* **84**, 2957 (2000).
18. J. Mydosh, *Spin Glasses: An Experimental Introduction* (Taylor and Francis, London, 1993).
19. Neutron diffraction experiments were performed on the Disc Chopper Spectrometer at NIST with 3.55-meV neutrons and an elastic energy resolution of 0.10 meV. Measurements versus T were carried out on the cold neutron triple axis spectrometer SPINS, with an energy of 5 meV and an energy resolution of 0.36 meV.
20. High degeneracy of low-temperature states is indicated not only by the large value of the entropy plateau at $S_M \approx \frac{1}{3} R \ln 3$ at $T \sim 20$ K but also by the stiffness constant D . For ordinary antiferromagnets that order at $T \sim |\theta_W|$, the stiffness D_0 is estimated by the relation $D_0^{-2} \approx [3/3\zeta(3)/4\pi](ak_B\theta_W/\hbar)^2/\ln(2S+1)$, with $\zeta(3) = 1.202$. In our case, the observed D was 850 m/s, nearly three times smaller than the expected D_0 of 2500 m/s, indicating softening due to magnetic frustration.
21. M. Imada, T. Mizusaki, S. Watanabe, available at <http://arxiv.org/abs/cond-mat/0307022> (2003).
22. T. Kashima, M. Imada, *J. Phys. Soc. Jpn.* **70**, 3052 (2001).
23. H. Kawamura, S. Miyashita, *J. Phys. Soc. Jpn.* **53**, 4138 (1984).
24. P. Chandra, P. Coleman, *Phys. Rev. Lett.* **66**, 100 (1991).
25. G. H. Wannier, *Phys. Rev.* **79**, 357 (1950).
26. M. F. Collins, O. A. Petrenko, *Can. J. Phys.* **75**, 605 (1997).
27. K. Takeda, K. Miyake, K. Takeda, K. Hirakawa, *J. Phys. Soc. Jpn.* **61**, 2156 (1992).
28. J. A. Wilson, in *Metallic and Nonmetallic States of Matter*, P. P. Edwards, C. N. R. Rao, Eds. (Taylor and Francis, London, 1985), pp. 215–260.
29. J. A. Beattie, *J. Math. Phys.* **6**, 1 (1926/1927).
30. We thank J. Y. Chan, S. Fujimoto, K. Ishida, K. Kitagawa, R. T. Macaluso, D. E. MacLaughlin, R. Moessner, S. Sondhi, and O. Tchernyshyov for fruitful discussions. Work at Kyoto University supported in part by Grants-in-Aid for Scientific Research from the Japan Society for the Promotion of Science and for the 21st Century Center of Excellence "Center for Diversity and Universality in Physics" from the Ministry of Education, Culture, Sports, Science and Technology (MEXT) of Japan and by the Inamori Foundation. Work at Johns Hopkins University was supported by the U.S. Department of Energy.

11 May 2005; accepted 4 August 2005
10.1126/science.1114727

Conversion of Zinc Oxide Nanobelts into Superlattice-Structured Nanohelices

Pu Xian Gao,¹ Yong Ding,¹ Wenjie Mai,¹ William L. Hughes,¹ Changshi Lao,¹ Zhong Lin Wang^{1,2,3*}

A previously unknown rigid helical structure of zinc oxide consisting of a superlattice-structured nanobelt was formed spontaneously in a vapor-solid growth process. Starting from a single-crystal stiff nanoribbon dominated by the c-plane polar surfaces, an abrupt structural transformation into the superlattice-structured nanobelt led to the formation of a uniform nanohelix due to a rigid lattice rotation or twisting. The nanohelix was made of two types of alternating and periodically distributed long crystal stripes, which were oriented with their c axes perpendicular to each other. The nanohelix terminated by transforming into a single-crystal nanobelt dominated by nonpolar (01 $\bar{1}$ 0) surfaces. The nanohelix could be manipulated, and its elastic properties were measured, which suggests possible uses in electromechanically coupled sensors, transducers, and resonators.

Helical structures have been observed for a number of inorganic materials. For example, carbon nanotube coils (1) are created when

paired pentagon-heptagon atomic rings arrange themselves periodically within the hexagonal carbon network (2). Formation of nanosprings

Magnetic Inversion Symmetry Breaking and Ferroelectricity in TbMnO_3

M. Kenzelmann,^{1,2,3} A. B. Harris,⁴ S. Jonas,³ C. Broholm,^{3,5} J. Schefer,² S. B. Kim,⁶ C. L. Zhang,⁶
S.-W. Cheong,⁶ O. P. Vajk,⁵ and J. W. Lynn⁵

¹Laboratory for Solid State Physics, ETH Hönggerberg, CH-8093 Zürich, Switzerland

²Laboratory for Neutron Scattering, ETH Zürich and Paul Scherrer Institute, CH-5232 Villigen, Switzerland

³Department of Physics and Astronomy, Johns Hopkins University, Baltimore, Maryland 21218, USA

⁴Department of Physics and Astronomy, University of Pennsylvania, Philadelphia, Pennsylvania 19104, USA

⁵NIST Center for Neutron Research, National Institute of Standards and Technology, Gaithersburg, Maryland 20899, USA

⁶Department of Physics & Astronomy, Rutgers University, 136 Frelinghuysen Rd., Piscataway, New Jersey 08854, USA

(Received 12 April 2005; published 19 August 2005)

TbMnO_3 is an orthorhombic insulator where incommensurate spin order for temperature $T_N < 41$ K is accompanied by ferroelectric order for $T < 28$ K. To understand this, we establish the magnetic structure above and below the ferroelectric transition using neutron diffraction. In the paraelectric phase, the spin structure is incommensurate and longitudinally modulated. In the ferroelectric phase, however, there is a transverse incommensurate spiral. We show that the spiral breaks spatial inversion symmetry and can account for magnetoelectricity in TbMnO_3 .

DOI: [10.1103/PhysRevLett.95.087206](https://doi.org/10.1103/PhysRevLett.95.087206)

PACS numbers: 77.80.Bh, 75.10.Jm, 75.25.+z, 75.40.Gb

The coexistence of antiferromagnetism and ferroelectricity in solid materials is rare, and much rarer still is a strong coupling between these two order parameters [1,2]. In nonmagnetic perovskites like BaTiO_3 , ferroelectricity is driven by a hybridization of empty d orbitals with occupied p orbitals of the octahedrally coordinated oxygen ions [3]. This mechanism requires empty d orbitals and thus cannot lead to magnetic ferroelectric materials. In materials such as BiMnO_3 , lone s^2 electron pairs can lower their energy by hybridizing with empty p orbitals [4]. While it leads to coexistence of magnetic order with electric polarization at low temperatures, the very different ordering temperatures show that the two order parameters lower the symmetry of the systems through distinctly different collective effects.

TbMnO_3 is an antiferromagnet which contains Mn^{3+} ions with occupied d orbitals and no lone s^2 cation [5]. So, as for a number of recently discovered multiferroics [6–8], neither of the mechanisms described above can explain the coexistence of magnetic and electric order. In these materials, a magnetic field of a few Tesla can switch the direction of the electric polarization [5]—proof of a strong direct coupling between the magnetic and electric polarization. Rare-earth manganese oxides show a plethora of exciting phenomena which arise from competing interactions. LaMnO_3 is the parent compound to a series of materials featuring colossal magnetoresistance, and shows orbital ordering of its e_g orbital, giving rise to layered antiferromagnetic ordering. With decreasing rare-earth size, there is a tendency towards incommensurate magnetic order. Ferroelectric ground states were recently predicted for doped manganites of the type $R_{1-x}\text{Ca}_x\text{MnO}_3$, but they have not yet been observed [9]. The coexistence and strong coupling of ferroelectricity and antiferromagnetism in TbMnO_3 suggests the presence of a nonconventional coupling mechanism involving competing spin interactions, and it is thus of both practical and fundamental importance.

To develop a microscopic theory of the new coupling mechanism, unambiguous determination of the symmetry of the magnetic order is essential. In this Letter, we present neutron diffraction measurements of orthorhombic TbMnO_3 , which determine the magnetic ground states and the phase diagram as a function of temperature and a magnetic field $\mathbf{H} \parallel \mathbf{a}$. We find that the ferroelectric phase transition coincides with a magnetic transition from a longitudinal incommensurate structure to an incommensurate spiral structure that breaks spatial inversion symmetry. We show that a recent theory proposed for axial-nonaxial parity breaking [10,11] predicts the observed orientation of the ferroelectric polarization based on the symmetry of the magnetic structure that we report.

TbMnO_3 crystals were grown using an optical floating zone furnace. A measurement of the temperature dependence of the dielectric constant of the two samples which we studied confirmed ferroelectricity below $T = 26$ K and $T = 28$ K for samples 1 and 2, respectively. The discrepancy may result from slightly differing oxygen partial pressure during annealing. The space group is No. 62, and in the Pbnm setting the lattice parameters are $a = 5.3$ Å, $b = 5.86$ Å, and $c = 7.49$ Å. The measurements were performed on two single-crystals weighing 40 and 220 mg, respectively, with the BT2 and SPINS spectrometers at NIST, and the TriCS 4-circle diffractometer at PSI.

The wave-vector dependence of the diffraction intensity along the $(0, k, 1)$ direction of reciprocal space (Figs. 1 and 2) illustrates the temperature dependence of magnetic order in TbMnO_3 . Mn^{3+} spins develop long-range order at $T_N = 41$ K [12,13]. Immediately below the transition temperature, magnetic Bragg peaks are observed at $(0, 1 - q, 1)$ and $(0, q, 1)$ positions. At 35 K the magnetic order is described by a single Fourier component associated with a wave vector $(0, q, 0)$ with $q = 0.27$, and no apparent higher-order Fourier components. Upon cooling below

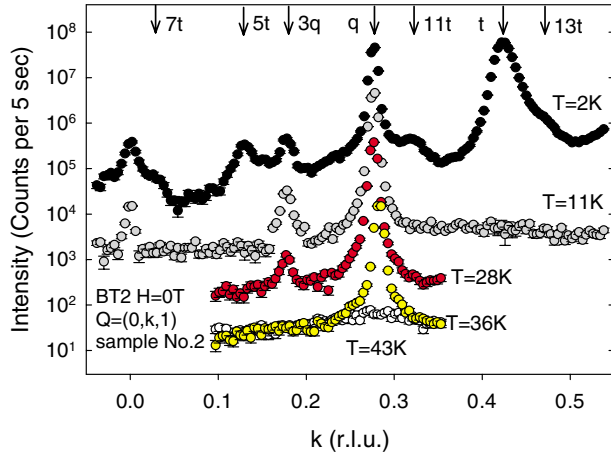


FIG. 1 (color online). Diffraction intensity along the $(0, k, 1)$ direction for different temperatures (with a factor 10 offset between the sub- T_N data sets), showing fundamental and higher-order Fourier components of the magnetic ordering. The $3t$ - and $9t$ -order peaks associated with the Tb order occur at $k = 0.725$ and 0.175 , respectively, and are difficult to identify unambiguously due to their proximity to strong peaks.

$T = 28$ K, third-order magnetic Bragg peaks $(0, 1 - 3q, 0)$ appear (Fig. 1), indicating steplike modulation of the magnetic moment. The inset to Fig. 2(b) shows that the wave vector continues to vary with temperature throughout the ferroelectric phase.

Below $T = 7$ K, additional magnetic peaks appear that are associated with Tb moments and indicate that their interactions favor a different ordering wave vector than for

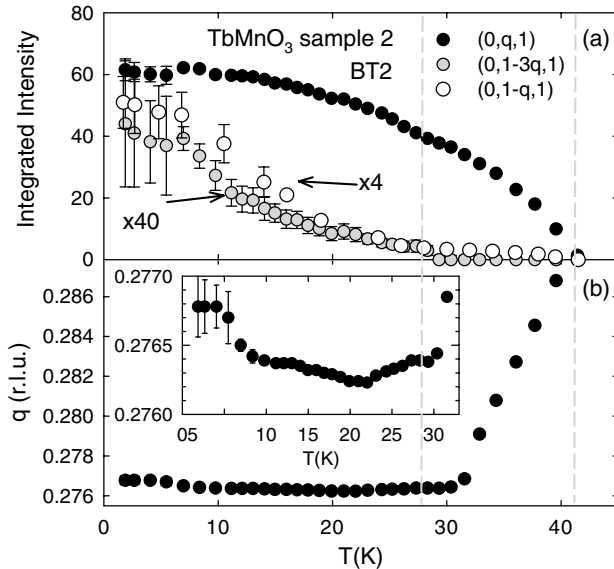


FIG. 2. (a) T dependence of the integrated intensity of the $(0, q, 1)$ Bragg peak and the associated third-order peak at $(0, 1 - 3q, 1)$. (b) T dependence of the wave vector q , corrected for the T dependence of the b lattice parameter, showing the absence of a lock-in transition at $T = 28$ K.

the Mn moments. At $T = 2$ K, there is a strong peak at $(0, t, 1)$ with $t = 0.425$, and several higher-order peaks as indicated in Fig. 1. The many strong odd high-order reflections indicate that the order associated with the $(0, t, 0)$ wave vector is strongly distorted (bunched structure) as expected for anisotropic rare-earth magnets. The correlation length and the incommensuration of the Tb order at low temperatures is sample dependent, as is often found in systems with phase transitions between incommensurate structures. The correlation length along the b axis was $58(20)$ and $280(20)$ Å, and t was 0.41 and 0.425 in samples 1 and 2, respectively.

The magnetic structures at $T = 15$ and 35 K were determined from up to 922 first-order magnetic Bragg peaks each. Only first-order peaks were included in the refinement as these are sufficient to determine the symmetry of the magnetic structure. Representational analysis was used to find the irreducible representations that describe the magnetic structures. The structure at $T = 35$ K in the high-temperature incommensurate (HTI) phase can be described by a single irreducible representation. The best fit with $\chi^2 = 0.86$ was obtained for a structure described by representation Γ_3 , and the excellent agreement between the model and the data is shown in Fig. 3(a). The magnetic structure is described by $\mathbf{m}_3^{\text{Mn}} = [0.0(8), 2.90(5), 0.0(5)]\mu_B$ and $\mathbf{m}_3^{\text{Tb}} = [0, 0, 0.0(4)]\mu_B$ where the subscript denotes the irreducible representation indicated in Fig. 4(c). The magnetic structure is longitudinally modulated with moment along the b axis, as illus-

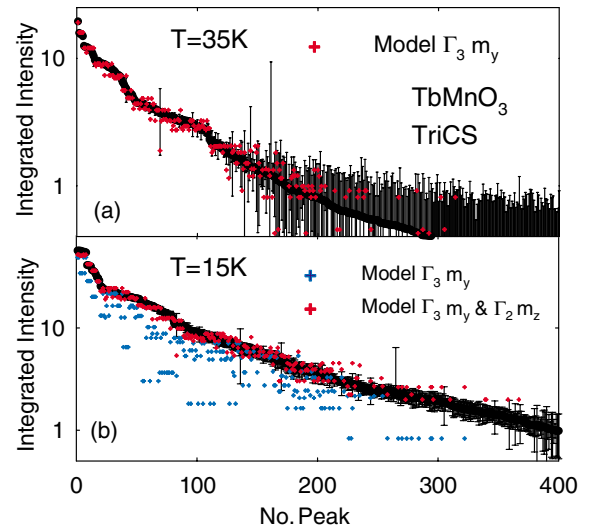


FIG. 3 (color). Integrated intensities of magnetic Bragg peaks measured at $T = 15$ K and $T = 35$ K using TriCS are compared to various magnetic structures. Peaks are sorted by decreasing measured intensity. (a) The $T = 35$ K structure is described by a single irreducible representation, Γ_3 , and the moments point along the b axis. (b) The $T = 15$ K magnetic structure is a spiral described by a y component of Γ_3 and an x component of Γ_2 with a $\pi/2$ phase shift.

trated in Fig. 4(a) and consistent with an earlier study [12]. The absence of observable higher-order peaks indicates that the magnetic structure at $T = 35$ K is sinusoidally modulated.

Two irreducible representations are required to describe the magnetic structure at $T = 15$ K in the low-temperature incommensurate (LTI) phase. We found best agreement with $\chi^2 = 2.19$ for magnetic ordering involving Γ_2 and Γ_3 , as shown in Fig. 3(b). Fits using the Γ_1 and Γ_3 , or the Γ_3 and Γ_4 representation pairs led to $\chi^2 = 14.5$ and higher, and can thus be excluded. Neglecting higher-order reflections, the magnetic structure is given by $\mathbf{m}_3^{\text{Mn}} = (0.0(5), 3.9(1), 0.0(7))\mu_B$, $\mathbf{m}_3^{\text{Tb}} = (0, 0, 0(1))\mu_B$, $\mathbf{m}_2^{\text{Mn}} = (0.0(1), 0.0(8), 2.8(1))\mu_B$, and $\mathbf{m}_2^{\text{Tb}} = (1.2(1), 0(1), 0)\mu_B$. The experiment was not sensitive to the phase between the y and z component of the Mn moment. From the size of the moment, however, we deduce that the Mn moments form an elliptical spiral. The data did not favor a phase difference between the Tb and Mn moments, so these phases remain undetermined. Symmetry splits the Tb moments into two orbits which representation theory normally treats as independent. However, as suggested by Landau theory [10], we took these two Tb amplitudes to be identical. The phase between the two orbits was found to be to $1.3(3)\pi$. The greatly improved fit is evidence that the Tb

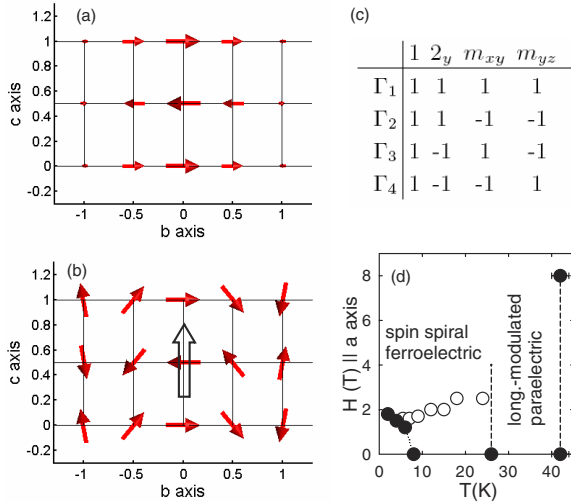


FIG. 4 (color online). Schematic of the magnetic structure at (a) $T = 35$ K and (b) $T = 15$ K, projected onto the b - c plane. Filled arrows indicate direction and magnitude of Mn moments. The longitudinally modulated phase (a) respects inversion symmetry along the c axis, but the spiral phase (b) violates it, allowing an electric polarization (unfilled arrow). (c) Irreducible representation of the group G_k for the incommensurate magnetic structure with $\mathbf{k} = (0, q, 0)$. (d) Phase diagram as a function of temperature and field applied along the a axis. Solid circles indicate second order phase transitions. Open circles indicate the characteristic field for reduction of magnetic $(0, 1 - q, 1)$ Bragg scattering from Tb moments by 50% from its zero-field intensity.

sublattice carries significant magnetization in the LTI phase, presumably as a consequence of the exchange field from the ordered Mn sublattice.

Figs. 5(a) and 5(b) show the field dependence of the $(0, q, 1)$ magnetic Bragg reflection, which arises from the Mn spin spiral. Both the position and the intensity are field independent to within errorbar—evidence that the structure remains a spiral up to at least 6 T. Our calculations show that the intensity should drop by 7% if the z component of Γ_2 were extinguished. In contrast, no decrease is observed to within an error bar of 2% between 0 and 6 T.

The $(0, 1 - q, 1)$ Bragg reflection shown in Fig. 5(a) arises from Mn Γ_3 magnetization along the a axis and from Tb Γ_2 magnetization along the a axis. Because the x component of the Mn moment is small, the $(0, 1 - q, 1)$ Bragg reflection is particularly sensitive to Tb order. For $T < 28$ K the $(0, 1 - q, 1)$ intensity is suppressed by a field $\mathbf{H} \parallel \mathbf{a}$ confirming that the modulated Tb moment is oriented along that direction. Below the Tb ordering temperature, the field dependent magnetic Bragg intensity has a finite-field maximum [Fig. 5(a)], indicating a spin-flop transition.

We collected 51 magnetic Bragg peaks at $T = 4$ K and $H = 4$ T along \mathbf{a} to determine the magnetic structure at low temperatures above the critical field for $(0, t, 0)$ Tb order [Fig. 5(c)]. The magnetic structure can be described by Γ_2 and Γ_3 with $\chi^2 = 3.81$ or by Γ_1 and Γ_3 with $\chi^2 = 4.19$. Since a field along the a direction disfavors anti-parallel spin alignment in the same direction as in the Γ_1 - Γ_3 structure, we infer that the structure is given by $\mathbf{m}_3^{\text{Mn}} = [0.3(4), 4.7(3), 0.0(5)]\mu_B$, $\mathbf{m}_3^{\text{Tb}} = [0, 0, 0.0(3)]\mu_B$, $\mathbf{m}_2^{\text{Mn}} = [0.0(2), 0.0(4), 3.0(3)]\mu_B$, and $\mathbf{m}_2^{\text{Tb}} = [0.3(2), 0.0(4), 0]\mu_B$. This result suggests that the spin spiral struc-

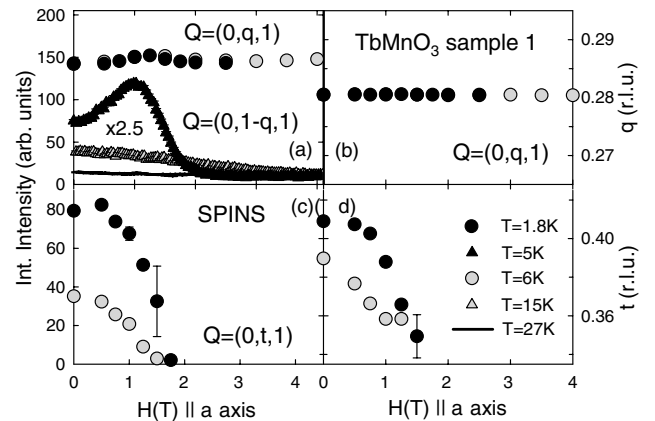


FIG. 5. Field dependence of magnetic Bragg scattering from TbMnO₃. (a) and (b) show data for the incommensurate peaks that occur for $T < 41$ K. (a) The $(0, q, 1)$ peak that is mostly sensitive to staggered magnetization on Mn sites and the $(0, 1 - q, 1)$ peak that is sensitive to staggered magnetization on Tb sites. (c) and (d) show data for the incommensurate peaks that develop for $T < 7$ K.

ture is more stable for fields along the a axis than for fields along the b axis [5].

Harris *et al.* [10,11] recently showed that insulators with axial-nonaxial parity breaking magnetic phase transitions must also be electrically polarized. Given the magnetic structure and the temperature dependence of the magnetic order parameter, the theory predicts the direction and temperature dependence of the electric polarization resulting from a symmetry allowed trilinear coupling term. In the following we show that this theory correctly accounts for the direction of the electric polarization in the LTI phase of TbMnO_3 , and the absence of electric polarization in the HTI phase. The trilinear magnetoelectric coupling term in the Landau free energy expansion is written as $V = \sum_{uv\gamma} a_{uv\gamma} \sigma_u(k) \sigma_v(-k) P_\gamma$. Here $\sigma_u(k)$ is the magnetic order parameter of irreducible representation Γ_u , P_γ is the electric polarization along the γ crystallographic direction and $a_{uv\gamma}$ parametrizes the strength of the interaction between the electric and magnetic order parameters. In the HTI phase, the magnetic order is described by only one irreducible representation, Γ_3 , and due to the high symmetry of the Mn moments, it is possible to define σ_u such that under inversion $\sigma_u(k) \rightarrow \sigma_u(k)^*$. The trilinear coupling thus consists only of terms such as $V = \sum_{\gamma} a_{\gamma} |\sigma_3(k)|^2 P_\gamma$. Since interactions in a Landau expansion must have the symmetry of the paramagnetic phase, this interaction must be invariant under inversion. This requires that a_γ vanishes, so that $P_\gamma = 0$ in the HTI phase. The conclusion remains valid for Tb order with no restriction on the phase between its two orbits.

For the LTI phase, which is described by Γ_2 and Γ_3 , there are, however, additional terms such as $V = \sum_{\gamma} b_{\gamma} \sigma_2(k) \sigma_3(-k) P_\gamma + \text{c.c.}$, where c.c. denotes the complex conjugate. For V to be an invariant, P_γ must transform as the product of Γ_2 and Γ_3 . That is, the electric polarization must be even under 1 and m_{yz} , and odd under 2_y and m_{xy} . This condition can only be satisfied for an electric polarization along the c axis. Previous dielectric experiments have shown that the electric polarization that develops below the transition to the LTI phase is indeed oriented along the c axis.

The coupling of the magnetic order parameter to electric polarization in TbMnO_3 [5] is similar to that in $\text{Ni}_3\text{V}_2\text{O}_8$, which adopts two different incommensurate magnetic structures [14], one of them ferroelectric and described by two irreducible representations. The correct prediction of the electric polarization for both TbMnO_3 and $\text{Ni}_3\text{V}_2\text{O}_8$ (Ref. [11]) suggests that magnetoelectricity resulting from a trilinear magnetoelectric coupling term may be commonplace in insulating transition metal oxides with noncollinear incommensurate structures. Accordingly we find less compelling the suggestion [5] that the appearance of ferroelectricity is associated with an incommensurate to commensurate phase transition. Indeed, there is no evidence of a lock-in transition [see Fig. 2(b)] and it therefore

appears to be irrelevant from the point of view of ferroelectricity whether the modulated magnetic order is commensurate or truly incommensurate.

In summary, we have determined the magnetic structure of the paraelectric and ferroelectric phases of TbMnO_3 . We have shown that the paraelectric, magnetically incommensurate phase has sinusoidally modulated collinear magnetic order that does not break inversion symmetry. The ferroelectric phase, however, has noncollinear incommensurate magnetic order described by two irreducible representations, which explicitly breaks inversion symmetry and thus gives rise to electric polarization. The qualitative aspects of magnetoelectric effects in TbMnO_3 appear to be accounted for by a trilinear coupling term in a Landau free energy expansion as proposed by Harris *et al.* [10,11]. Understanding the magnitude of the effect will require experimental as well as theoretical work to track lattice, charge, and orbital degrees of freedom through axial-nonaxial parity breaking phase transition in insulators such as TbMnO_3 . Apart from the fundamental challenge, improved understanding of magnetoelectricity in these systems may help to produce materials for room-temperature applications.

We thank A. Aharony, O. Entin-Wohlman, and A. Ramirez for helpful discussions. This work was supported by the Swiss National Science Foundation under Contract No. PP002-102831. Work at Johns Hopkins University was supported by the DoE through DE-FG02-02ER45983. Work at University of Pennsylvania and Johns Hopkins University was supported in part by the U.S.-Israel Binational Science Foundation under Grant No. 2000073. Work at Rutgers University was supported by the NSF-DMR-MRSEC-05-20471. This work is based on experiments performed at the Swiss spallation neutron source SINQ, Paul Scherrer Institute, Villigen, Switzerland. The work at SPINS is based upon activities supported by the National Science Foundation under Agreement No. DMR-9986442.

-
- [1] G. A. Smolenskii *et al.*, Sov. Phys. Usp. **25**, 475 (1982).
 - [2] H. Schmid, Ferroelectrics **62**, 317 (1994).
 - [3] R. E. Cohen, Nature (London) **358**, 136 (1992).
 - [4] M. Atanasov *et al.*, J. Phys. Chem. A **105**, 5450 (2001).
 - [5] T. Kimura *et al.*, Nature (London) **426**, 55 (2003).
 - [6] T. Lottermoser *et al.*, Nature (London) **430**, 541 (2004).
 - [7] N. Hur *et al.*, Nature (London) **429**, 392 (2004).
 - [8] S. Kobayashi *et al.*, J. Phys. Soc. Jpn. **73**, 1593 (2004).
 - [9] D. V. Efremov *et al.*, Nat. Mater. **3**, 853 (2004).
 - [10] A. B. Harris *et al.* (to be published).
 - [11] G. Lawes *et al.*, Phys. Rev. Lett. **95**, 087205 (2005).
 - [12] S. Quezel *et al.*, Physica (Amsterdam) **86B-88B**, 916 (1977).
 - [13] R. Kajimoto *et al.*, Phys. Rev. B **70**, 012401 (2004).
 - [14] G. Lawes *et al.*, Phys. Rev. Lett. **93**, 247201 (2004).

Inhomogeneous Level Splitting in $\text{Pr}_{2-x}\text{Bi}_x\text{Ru}_2\text{O}_7$

J. van Duijn,^{1,2} K. H. Kim,^{3,*} N. Hur,⁴ D. Adroja,² M. A. Adams,² Q. Z. Huang,⁵ M. Jaime,³ S.-W. Cheong,⁴
C. Broholm,^{1,5} and T. G. Perring²

¹*Department of Physics and Astronomy, Johns Hopkins University, Baltimore, Maryland 21218, USA*

²*ISIS Facility, Rutherford Appleton Laboratory, Chilton, Didcot, OX11 0QX, United Kingdom*

³*MST-NHML, Los Alamos National Laboratory, New Mexico 87544, USA*

⁴*Department of Physics and Astronomy, Rutgers University, Piscataway, New Jersey 08854, USA*

⁵*NIST Centre for Neutron Research, National Institute of Standards and Technology, Gaithersburg, Maryland 20899, USA*

(Received 4 October 2004; published 2 May 2005; corrected 5 May 2005)

We report that Bi doping drives $\text{Pr}_{2-x}\text{Bi}_x\text{Ru}_2\text{O}_7$ from an antiferromagnetic insulator ($x = 0$) to a metallic paramagnet ($x \approx 1$) with a broad low T maximum in C/T . Neutron scattering reveals local low energy spin excitations ($\hbar\omega \approx 1$ meV) with a spectrum that is unaffected by heating to $k_B T \gg \hbar\omega$. We show that a continuous distribution of splittings of the non-Kramers Pr^{3+} ground-state doublet such as might result from various types of lattice strain can account for all the data.

DOI: 10.1103/PhysRevLett.94.177201

PACS numbers: 75.10.Dg, 71.27.+a, 71.70.Fk

Rare earth ions with an even number of electrons in a partially filled $4f$ shell require a highly symmetric environment to retain ground-state degeneracy. Such non-Kramers degeneracy is consequently unstable towards lattice distortions, which can occur spontaneously through the Jahn-Teller effect, dynamically through interactions with phonons [1], or at random due to static inhomogeneities [2]. In this Letter we describe an inadvertent encounter with the latter effect while exploring the unusual thermomagnetic properties of a diluted frustrated magnet, $\text{Pr}_{2-x}\text{Bi}_x\text{Ru}_2\text{O}_7$. While the enhanced specific heat of the material is reminiscent of ultraheavy fermion behavior, the temperature (T) and wave vector (Q) independent neutron spectra and the diverging susceptibility implicate inhomogeneous level splitting of the non-Kramers Pr doublet. Our comprehensive analysis links neutron, specific heat, and susceptibility data and is important because similar physics may be operative in other magnets of recent notoriety.

The parent material, $\text{Pr}_2\text{Ru}_2\text{O}_7$, contains two sublattices of magnetic ions on the vertices of corner-sharing tetrahedra. This lattice is notable because antiferromagnetic nearest neighbor interactions do not select a unique long range ordered spin configuration but a highly degenerate manifold. While $\text{Pr}_2\text{Ru}_2\text{O}_7$ does develop magnetic order at $T_N = 165$ K, dilution of the Pr^{3+} sites by the smaller isovalent Bi^{3+} ion converts the ordered insulator to a metallic paramagnet. Similar behavior was found in other rare earth ruthenates; however, the Pr based material has a greatly enhanced low- T specific heat with analogies to non-Fermi-liquid and heavy fermion systems. Here we link the anomalies to static inhomogeneous splitting of the non-Kramers Pr^{3+} doublet, and consider various options to account for the inhomogeneity.

Powdered samples of $\text{Pr}_{2-x}\text{Bi}_x\text{Ru}_2\text{O}_7$ were synthesized by the solid state reaction method. The mixtures of Pr_2O_3 , Bi_2O_3 , and RuO_2 in proper molar ratios were prereacted at 850°C for 15 h in air and then ground and pressed into pellets. The pellets were sintered at $1000\text{--}1200^\circ\text{C}$ in air

with intermediate grindings. Powder x-ray diffraction measurements indicated single phase samples. Powder neutron diffraction data were collected on a $x \approx 1.0$ sample, using the BT1 diffractometer at NIST. Rietveld analysis confirmed the cubic pyrochlore structure and inductively coupled plasma-emission spectroscopy showed the Pr:Bi composition to be 1:0.94 corresponding to $x = 0.97$. This sample was subsequently used for inelastic neutron scattering experiments.

Zero field heat capacity measurements were carried out on all members of the series using a commercial calorimeter. Field dependent heat capacity measurements employed a homemade probe with a Si platform in a superconducting magnet. The electrical resistivity, ρ , of the polycrystalline samples was measured by the four-probe method. The overall temperature dependence of ρ for different doping levels, x , are similar to those reported for $\text{Y}_{2-x}\text{Bi}_x\text{Ru}_2\text{O}_7$ [3,4]. $\text{Pr}_2\text{Ru}_2\text{O}_7$ ($x = 0$) is insulating while $\text{Bi}_2\text{Ru}_2\text{O}_7$ ($x = 2$) is metallic (Fig. 1). For intermediate values of x , ρ decreases abruptly with x indicating an insulator to metal transition for $x \approx 0.8$.

Magnetic susceptibility data were collected on selected samples using a SQUID magnetometer. The insulating $x = 0$ sample shows abrupt development of hysteresis for $T < T_N = 165$ K indicating Néel order plus spin canting from anisotropic exchange interactions [5,6]. While the $x = 2$ sample behaves as a Pauli paramagnet [4], samples near the metal insulator transition for $x \approx 0.8$ have an increasing susceptibility upon cooling but fail to develop magnetic order down to $T = 1.5$ K (Fig. 2).

Figure 1(a) shows that metallic $\text{Pr}_{2-x}\text{Bi}_x\text{Ru}_2\text{O}_7$ samples close to the metal insulator transition have a strongly enhanced low- T specific heat, $C(T)$. In this figure the lattice contributions have been subtracted using data from the $x = 2$ sample corrected for unit cell mass through the Debye interpolation scheme. For $x = 0.8$ and $T \approx 2.0$ K the specific heat ($C/T = 0.7$ J/mole f.u./K²) is more than 3 orders of magnitude greater than for a con-

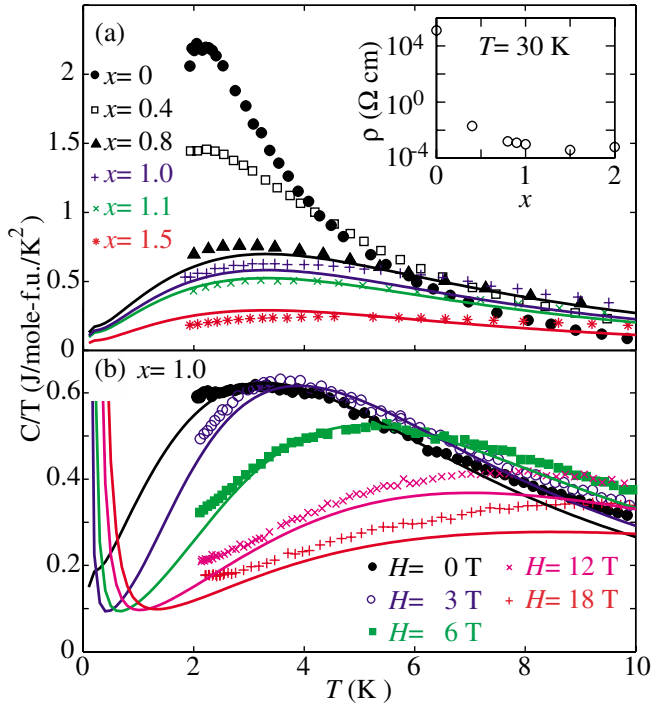


FIG. 1 (color online). Temperature dependence of the specific heats C/T of $\text{Pr}_{2-x}\text{Bi}_x\text{Ru}_2\text{O}_7$ (a) for various x and $H=0$, and (b) for various fields (H) for $x=1.0$. The lattice contribution was subtracted as described in the text. The solid lines show C/T calculated from the observed neutron spectra and the assumption of a quenched level distribution [Eq. (3)]. A γ term of 0.04 J/mole/K² was added to the model in (b). Inset: electrical resistivity, ρ , of various x at 30 K.

ventional metal. Figure 1(b) shows that the enhanced specific heat is very sensitive to a magnetic field indicating a high density of magnetic states.

To determine their origin we performed inelastic neutron scattering experiments on the HET and IRIS spectrometers at the ISIS Facility. On HET we used incident energies of $E_i = 35$ and 160 meV, which produced an elastic energy resolution of 1.4 and 7 meV, respectively. For the IRIS experiment disk choppers selected an incident energy spectrum from 1.3 to 4.6 meV pulsed at 25 Hz and a backscattering pyrolytic graphite analyzer system with a 25 K Be filter selected a final energy of $E_f = 1.847$ meV for an elastic energy resolution of 17.5 μeV . Count rates were normalized to the incoherent scattering from a vanadium slab for the HET experiment, while IRIS data were normalized using coherent nuclear scattering from the sample. These procedures yield absolute measurements of $\tilde{I}(Q, \hbar\omega) = (\gamma r_0)^2 |\frac{g}{2} F(Q)|^2 2S(Q, \hbar\omega)$ to an overall scale accuracy of 20% . Here $\gamma = -1.913$ and g are spectroscopic g factors of the neutron and magnetic ion, respectively, $r_0 = 2.82$ fm is the classical electron radius, $F(Q)$ is the magnetic form factor for Pr [7], and $S(Q, \hbar\omega)$ is the spherically averaged dynamic correlation function [8,9].

To determine the relevant low energy degrees of freedom, we used inelastic neutron scattering to map the

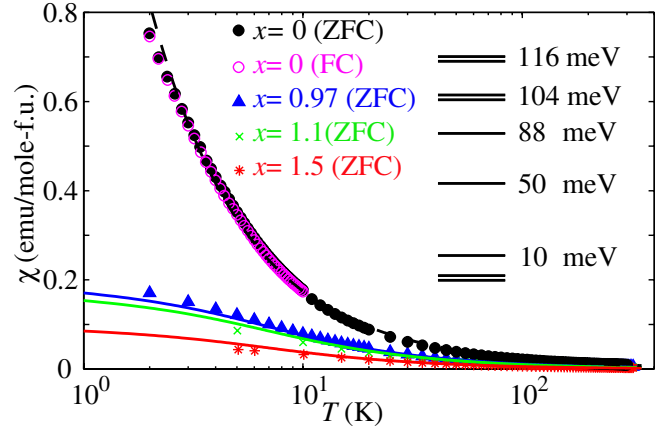


FIG. 2 (color online). Temperature dependence of the magnetic susceptibility χ of $\text{Pr}_{2-x}\text{Bi}_x\text{Ru}_2\text{O}_7$ for various x . The solid lines show the calculated magnetic susceptibility defined as $\chi(T) = \chi'(T) + \chi_{\text{CF}}(T)$. Here $\chi'(T)$ is given by Eq. (4) and $\chi_{\text{CF}}(T)$ is the contribution from the higher energy CF levels. The dashed line shows the calculated susceptibility for a doublet ground state. Inset: the Pr^{3+} CF energy level scheme.

crystal field (CF) level scheme for Pr^{3+} in the sample. Five magnetic excitations were identified at $9.5(1)$, $50(5)$, $84.0(1)$, $103.1(1)$, and $115.7(2)$ meV [9]. The number of excitations is consistent with a $J = 4$ ion in D_{3d} symmetry. The fact that excitations are observed in all five excited states implies a doublet ground state. Further analysis of the spectrum indicates a ground-state wave function of the form $|\pm\rangle = \alpha|\mp 4\rangle + \beta|\pm 2\rangle \pm \gamma|\mp 1\rangle$, where $\alpha = 0.90(4)$, $\beta = -0.10(3)$, and $\gamma = 0.42(7)$. CF excitations in the bismuth doped sample were broadened considerably as compared to pure $\text{Pr}_2\text{Ru}_2\text{O}_7$ where the excitations are almost resolution limited. The average doping induced half width at half maximum of 3.8 meV is a first indication of a distribution of CF environments.

The low energy magnetic response in the $x = 1.0$ sample features a broad and apparently dispersionless peak centered at ~ 1 meV energy transfer (Figs. 3 and 4). The large spectral weight and the low energy scale suggests that these excitations are related to the enhanced low- T specific heat of the material. The wave vector dependence of the intensity follows the squared single ion form factor of Pr^{3+} (Fig. 3), indicating an absence of correlations between Pr sites and single ion physics. This is unusual for a dense Kondo (lattice) system, as, in general, competition between intersite RKKY and on-site Kondo singlet formation produces short range antiferromagnetic correlations. The data also appear to be inconsistent with isolated Kondo singlets, which cannot scatter inelastically as $Q \rightarrow 0$ [10–12]. Most revealing, however, is that the spectrum, when appropriately scaled (Fig. 4), is utterly unaffected by heating to temperatures of order the Néel temperature for the parent insulator. This unusual result indicates that the finite width of the sample averaged spectrum results from some form of quenched inhomogeneity rather than relaxation effects.

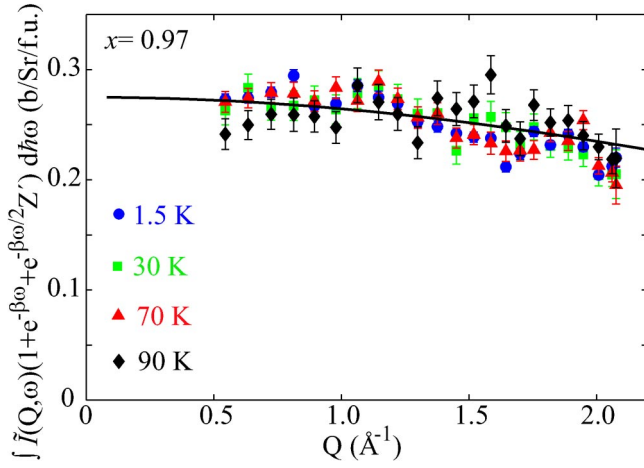


FIG. 3 (color online). Q dependence of energy integrated inelastic neutron scattering intensity for $T = 15, 30, 70$, and 90 K. Data were obtained by integrating over $0.5 \leq \hbar\omega \leq 1.5$ meV. The solid line shows $|F(Q)|^2$ for Pr^{3+} scaled to the data [7].

We now pursue such an explanation for low energy physics in $\text{Pr}_{2-x}\text{Bi}_x\text{Ru}_2\text{O}_7$ more carefully. As Pr^{3+} is a non-Kramers ion, a doublet ground state relies on D_{3d} point group symmetry. Lowering of the CF symmetry with an amplitude that varies through the sample would split the doublet by varying amounts on different sites. Such quenched inhomogeneity would produce a T independent spectrum of singlet-singlet transitions. As it is based on single site CF dynamics, this explanation links neutron scattering, specific heat, and susceptibility data in a parameter-free fashion that we shall put to the test.

Denote the quenched distribution of singlet-singlet splitting by $\rho(\Delta)$ such that $N\rho(\Delta)d\Delta$ is the number of Pr ions with level splitting between Δ and $\Delta + d\Delta$ and N is the total number of formula units in the sample. Using expressions for the generalized susceptibility of the CF split doublet and the fluctuation dissipation theorem [8], it is straightforward to show that the splitting distribution function is related to the sample averaged response functions as follows:

$$\rho(\hbar\omega) = \frac{\chi''(\hbar\omega)}{\pi(g\mu_B\alpha)^2} \frac{1 + e^{-\beta\hbar\omega} + e^{-\beta\hbar\omega/2}Z'(\beta)}{1 - e^{-\beta\hbar\omega}} \quad (1)$$

$$= \frac{1}{\alpha^2} S(\hbar\omega) [1 + e^{-\beta\hbar\omega} + e^{-\beta\hbar\omega/2}Z'(\beta)]. \quad (2)$$

Here $\beta = 1/k_B T$, χ'' denotes the imaginary part of the generalized susceptibility, $g = 0.8$ is the spectroscopic g factor for Pr^{3+} , α^2 is the powder averaged squared singlet-singlet matrix element [13], and $Z'(\beta) = \sum_i n_i e^{-\beta E_i}$ is the partition sum excluding the low energy doublet. Figure 4 shows $(g/2)^2 S(\hbar\omega) [1 + e^{-\beta\hbar\omega} + e^{-\beta\hbar\omega/2}Z'(\beta)]$, which according to Eq. (1) and the underlying assumptions should be T independent. The excellent data collapse

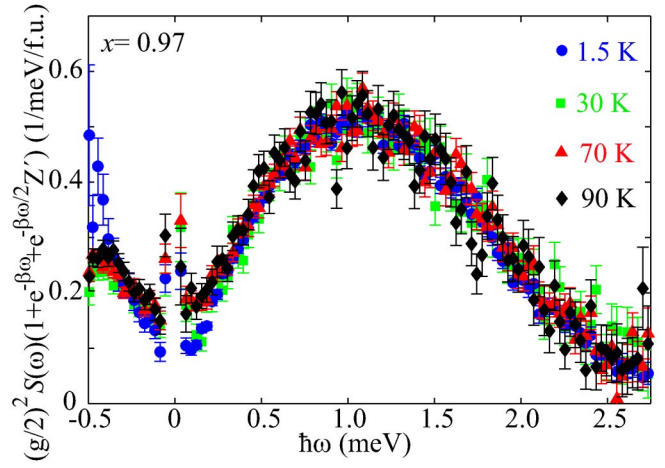


FIG. 4 (color online). Energy dependence of Q -averaged neutron scattering data scaled for proportionality to the level distribution function, $\rho(\Delta)$ of Eq. (1). The data collapse indicates that $\rho(\Delta)$ is T independent in the range probed.

provides strong evidence that the observed spectrum, indeed, results from inhomogeneous splitting of the Pr CF doublet. While the discrepancy at negative energies results from incomplete background subtraction, the differences in the data for $\hbar\omega \approx 0.1$ meV can be ascribed to incoherent inelastic phonon scattering on account of the approximately linear T dependence.

Using perturbation theory and Eq. (1), the T dependence of the specific heat and magnetic susceptibility can now be obtained directly from the neutron results for $\rho(\Delta)$ with *no* adjustable parameters.

$$C_p(H, T) = k_B \int \frac{d\Omega_H}{4\pi} \times \int_0^\infty \rho(\Delta) (\beta \Delta(H_z))^2 \frac{e^{\beta \Delta(H_z)}}{(1 + e^{\beta \Delta(H_z)})^2} d\Delta, \quad (3)$$

$$\chi'(T) = 2(g\mu_B\alpha)^2 \int_0^\infty \frac{\rho(\Delta)}{\Delta} \times \frac{1 - e^{-\beta\Delta}}{1 + e^{-\beta\Delta} + e^{-\beta\Delta/2}Z'(\beta)} d\Delta. \quad (4)$$

Here $\Delta(H_z)^2 = (2g\mu_B H_z \langle + | J_z | + \rangle)^2 + \Delta^2$ and H_z is the component of the magnetic field along the local threefold axis. Note that Eq. (4) becomes the exact Kramers-Kronig relation when $\rho(\Delta)$ from Eq. (1) is evaluated at the running temperature. However, the assumption of a quenched distribution backed by Fig. 4 allows calculation of the full temperature dependence of $\chi'(T)$ based on a single neutron spectrum. To minimize contributions from phonon scattering we used $T = 1.5$ K data to derive $\rho(\Delta)$. Note, however, that indistinguishable results are obtained using the average of all temperatures.

The lines in Fig. 1 were calculated from Eq. (3) neglecting any variation of $\rho(\Delta)$ with Pr concentration. We added

the nuclear specific heat as calculated from the natural isotope distribution of the sample [14]. In the bottom frame we added a common best fit Sommerfeld term, $\gamma_{\text{Ru}} = 40 \text{ mJ/mole/K}^2$, to account for contributions from the metallic state. This value is not dissimilar from $\gamma_{\text{Ru}} = 72 \text{ mJ/mole/K}^2$ for Pauli paramagnetic YBiRu_2O_7 . The magnetic susceptibility was calculated as $\chi(T) = \chi'(T) + \chi_{\text{CF}}(T)$, where $\chi'(T)$ is given by Eq. (4) and $\chi_{\text{CF}}(T)$ accounts for contributions from higher energy CF levels [15]. The discrepancy between the lines and the data points is of order the accuracy in the overall normalization of the specific heat, susceptibility, and neutron data. As there are *no* adjustable parameters, this supports the inference that Pr ions in $\text{Pr}_{2-x}\text{Bi}_x\text{Ru}_2\text{O}_7$ form a distributed two level system.

The measured distribution function provides important clues to the origin of level splitting in $\text{Pr}_{2-x}\text{Bi}_x\text{Ru}_2\text{O}_7$. The absence of T dependence to $\rho(\Delta)$ from 1.5 to 90 K (see Fig. 4) all but rules out dynamic phenomena. Fluctuations slow enough to be quasistatic on the time scale of the $\approx 1 \text{ meV}$ singlet-singlet transitions would be thermally activated in that temperature range. So rather than reflecting changes with time for a single Pr ion, $\rho(\Delta)$ represents a spatial distribution of Pr environments. Because Eq. (3) accounts for finite field data too, magnetostatic disorder from high T Ru spin freezing seems unlikely, though this deserves further examination through muon spin relaxation (μSR) measurements. To produce a continuous distribution rather than a finite set of levels, the length scale associated with this disorder must greatly exceed the lattice spacing. Possible mechanisms include a low density of extended defects or a density wave which generates a continuum of local environments. The natural culprit would be Bi doping; however, this would appear to be at odds with the fact that a single distribution function measured for $x = 0.97$ accounts for all specific heat data for $x > 0.8$. There are, in fact, indications of disorder for both end members of the series. While the high T specific heat anomaly for $\text{Pr}_2\text{Ru}_2\text{O}_7$ indicates quasi-long-range Néel order below $T_N(\text{Ru}) = 165 \text{ K}$, the phase transition is accompanied by a difference in the field cooled and zero field cooled susceptibility. Furthermore, with a residual resistivity of $1.5 \text{ m}\Omega \text{ cm}$ the metallic end member, $\text{Bi}_2\text{Ru}_2\text{O}_7$ appears to be severely disordered. These results suggest that a common low density of large defects principally controlled by the ruthenium sublattice may influence $\text{Pr}_{2-x}\text{Bi}_x\text{Ru}_2\text{O}_7$ at least through the metallic part of the phase diagram.

Pyrochlore systems are, indeed, known to suffer from various types of clandestine disorder. $\text{Y}_2\text{Mo}_2\text{O}_7$ was, for example, recently shown to have significant disorder on the Mo sublattice [16]. Virtually undetectable through diffraction, this quenched disorder nonetheless causes spin freezing for $T < T_g = 22.5 \text{ K}$. Just as non-Kramers doublets are particularly sensitive to disorder, so are highly frustrated magnets so that modest levels of disorder that might

not affect more conventional magnetic materials can have qualitative effects in these systems. Materials such as $\text{Pr}_{2-x}\text{Bi}_x\text{Ru}_2\text{O}_7$ and $\text{Pr}_2\text{Ir}_2\text{O}_7$ [17] that are *both* magnetically frustrated *and* contain a non-Kramers ion are particularly susceptible to these effects.

Non-Kramers magnetic ions include Pr^{3+} , Pm^{3+} , Sm^{2+} , Eu^{3+} , Tb^{3+} , Ho^{3+} , and Tm^{3+} from the rare earth series and U^{4+} from the actinides. There are a number of materials of current interest where distributed lifting of non-Kramers degeneracies might account for unusual low- T anomalies. These include nominally stoichiometric materials such as $\text{Tb}_2\text{Ti}_2\text{O}_7$ [18] and $\text{Ho}_2\text{Ti}_2\text{O}_7$ [19]. There may also be specific interesting effects of doping non-Kramers systems as in $\text{LiHo}_x\text{Y}_{1-x}\text{F}_4$ [20] and $\text{Tb}_x\text{Y}_{2-x}\text{Ti}_2\text{O}_7$ [21] where symmetry breaking impurities may act as a random transverse field.

It is a pleasure to acknowledge O. Tchernyshyov and B.D. Rainford for helpful discussions, as well as A. Migliori for his assistance. The work at JHU and ISIS was supported by DOE through Grant No. DE-FG02-02ER45983. The work at Rutgers was supported by NSF through Grant No. DMR-0103858. K.H.K. was partially supported by KOSEF through CSCMR.

*Permanent address: CSCMR & School of Physics, Seoul National University, Seoul 151-747, S. Korea.

- [1] A. T. Boothroyd *et al.*, Phys. Rev. Lett. **86**, 2082 (2001).
- [2] G. Carini *et al.*, Philos. Mag. B **77**, 449 (1998).
- [3] R. Kanno *et al.*, J. Solid State Chem. **102**, 106 (1993).
- [4] S. Yoshii and M. Sato, J. Phys. Soc. Jpn. **68**, 3034 (1999).
- [5] N. Taira, M. Wakeshima, and Y. Hinatsu, J. Phys. Condens. Matter **11**, 6983 (1999).
- [6] N. Taira, M. Wakeshima, and Y. Hinatsu, J. Solid State Chem. **152**, 441 (2000).
- [7] P.J. Brown, in *International Tables for Crystallography*, edited by A. J. C. Wilson (Kluwer, London, 1995), Vol. C.
- [8] S.W. Lovesey, *Theory of Neutron Scattering from Condensed Matter* (Clarendon Press, Oxford, 1984).
- [9] J. van Duijn *et al.*, Phys. Rev. B (to be published).
- [10] A.P. Murani, Phys. Rev. B **50**, 9882 (1994).
- [11] D.T. Adroja *et al.*, Phys. Rev. B **68**, 094425 (2003).
- [12] E.A. Goremychkin *et al.*, Phys. Rev. Lett. **84**, 2211 (2000); E.A. Goremychkin *et al.*, Phys. Rev. Lett. **89**, 147201 (2002).
- [13] S.K. Malik, J. Tang, and K.A. Gschneidner Jr., J. Magn. Magn. Mater. **109**, 316 (1992).
- [14] E.R. Gopal, *Specific Heats at Low Temperatures* (Heywood Books, London, 1966).
- [15] J. Jensen, J. Magn. Magn. Mater. **29**, 47 (1982).
- [16] C. Booth *et al.*, Phys. Rev. B **62**, R755 (2000).
- [17] D. Yanagishima and Y. Maeno, J. Phys. Soc. Jpn. **70**, 2880 (2001).
- [18] J.S. Gardner *et al.*, Phys. Rev. Lett. **82**, 1012 (1999).
- [19] M.J. Harris *et al.*, Phys. Rev. Lett. **79**, 2554 (1997).
- [20] J. Brooke *et al.*, Science **284**, 779 (1999).
- [21] A. Keren *et al.*, Phys. Rev. Lett. **92**, 107204 (2004).

Crystalline electric field levels and magnetic properties of the metallic pyrochlore compound $\text{Pr}_2\text{Ir}_2\text{O}_7$

Y. Machida^{a,*}, S. Nakatsuji^a, H. Tonomura^a, T. Tayama^b, T. Sakakibara^b, J. van Duijn^{c,d},
C. Broholm^d, Y. Maeno^{a,e}

^aDepartment of Physics, Kyoto University, Kyoto 606-8502, Japan

^bInstitute of Solid State Physics (ISSP), University of Tokyo, Kashiwa 277-8581, Japan

^cISIS Facility, Rutherford Appleton Laboratory, Oxfordshire OX11 0QX, UK

^dDepartment of Physics and Astronomy, Johns Hopkins University, Baltimore, MD 21218, USA

^eInternational Innovation Center, Kyoto University, Kyoto 606-8501, Japan

Abstract

DC susceptibility, specific heat and inelastic neutron scattering measurements have been performed on the metallic pyrochlore compound $\text{Pr}_2\text{Ir}_2\text{O}_7$. No anomalies indicative of a magnetic phase transition were found for temperatures greater than 1.8 K. Our experiments and analysis show that Pr^{3+} ground state is a well-isolated magnetic doublet with Ising-like moments of $\sim 3.0 \mu_B$ oriented along the local $\langle 111 \rangle$ direction of each tetrahedral unit.

© 2005 Elsevier Ltd. All rights reserved.

1. Introduction

Pyrochlore oxides of the form $\text{A}_2\text{B}_2\text{O}_7$ have attracted much interest because of their unique physical properties. Both the A and B sites individually form sublattice of corner-sharing tetrahedron (Fig. 1), and if either A or B site is occupied by a magnetic ion, the magnetic interactions are highly frustrated. Ferromagnetic interactions plus strong Ising anisotropy can induce a frustrated frozen state called the ‘spin ice’ [1]. An isotropic spin system on a pyrochlore lattice with nearest neighbor antiferromagnetic exchange should have a spin liquid ground state [2], which however, is fragile toward various types of sub-leading interactions that can lead to spin freezing or long-range order.

Recently, ‘spin liquid’ or ‘cooperative paramagnetism’ has been discovered in an insulating antiferromagnet pyrochlore $\text{Tb}_2\text{Ti}_2\text{O}_7$ compound [3]. In this system, Tb^{3+} moments fluctuate down to 50 mK, despite an antiferromagnetic Curie–Weiss (CW) temperature of 20 K. The neutron spin echo measurement revealed that the majority

of the spins fluctuate very rapidly even at 50 mK, and spatial correlations do not develop beyond nearest neighbor [4].

Pyrochlore iridates $\text{R}_2\text{Ir}_2\text{O}_7$ ($\text{R} = \text{Y}$, rare earth elements) are particularly interesting because they exhibit an insulator to metal transition with increasing R^{3+} ionic radius. Among these compounds, $\text{Pr}_2\text{Ir}_2\text{O}_7$ is metallic and remains paramagnetic down to 0.3 K, despite indications of localized Pr moments [5]. $\text{Pr}_2\text{Ir}_2\text{O}_7$ therefore offers a novel opportunity of exploring a possible spin liquid state embedded in a metal.

The purpose of this paper is to determine the Pr^{3+} single-ion ground state in $\text{Pr}_2\text{Ir}_2\text{O}_7$. Our dc susceptibility and specific heat measurements indicate that the crystalline electric field (CEF) ground state is a doublet. We have furthermore determined the CEF energy level scheme through inelastic neutron scattering from $\text{Pr}_2\text{Ir}_2\text{O}_7$ powder sample.

2. Experimental

Polycrystalline samples of $\text{Pr}_2\text{Ir}_2\text{O}_7$ was prepared by firing Pr_6O_{11} , Y_2O_3 and IrO_2 powders at 1100 °C in air for several days. Powder X-ray diffraction patterns of the samples showed that they are single phases. Single-crystals of $\text{Pr}_2\text{Ir}_2\text{O}_7$ with a volume of 1 mm³ were grown by a flux

* Corresponding author. Tel.: +81 75 753 3793.

E-mail address: machida@scphys.kyoto-u.ac.jp (Y. Machida).

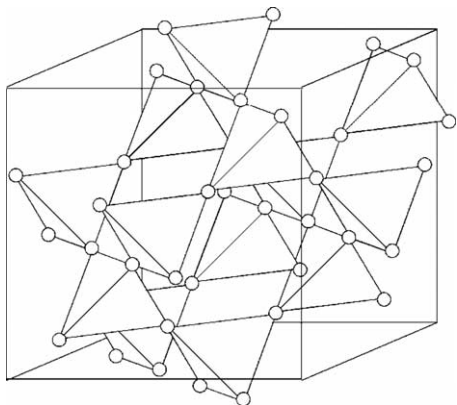


Fig. 1. Pyrochlore lattice of corner-sharing tetrahedra.

method using high quality polycrystalline starting materials as described elsewhere [6].

DC susceptibility data were acquired between 1.8 and 350 K in fields up to 7 T using a SQUID magnetometer (Quantum Design, MPMS-XL). High-field magnetization measurements up to 13 T were performed using a capacitive Faraday-force magnetometer at ISSP, Kashiwa, Japan. Specific heat measurements were performed using a thermal relaxation method (Quantum Design, PPMS) in the temperature range of 0.3–300 K. Inelastic neutron scattering measurements were performed using high quality powder samples of $\text{Pr}_2\text{Ir}_2\text{O}_7$ at the HET spectrometer of the ISIS facility. The incident energy was either 35 or 160 meV and we used high angle spectra and multiple scattering analysis to isolate magnetic scattering from the low angle spectra.

3. Results and discussion

Fig. 2 shows the inverse susceptibility $(\chi - \chi_0)^{-1}$ of $\text{Pr}_2\text{Ir}_2\text{O}_7$ at an applied field of 0.1 T along [111] direction. Here, χ_0 is the temperature independence term determined by the following Curie–Weiss (CW) analysis. The CW analysis [$\chi = \chi_0 + C/(T - \theta_{\text{CW}})$] between 100 and 350 K yields χ_0 of 1.25×10^{-3} emu/mol-Pr and an effective moment of $3.05 \mu_{\text{B}}/\text{Pr}^{3+}$, which corresponds to $g_J J$ of $2.68 \mu_{\text{B}}/\text{Pr}^{3+}$. Here, g_J represents Lande's g factor, J corresponds to the total angular momentum, and μ_{B} represents the Bohr magneton. The temperature independent term χ_0 is supposed to come from Ir^{4+} moments. In fact, the above χ_0 has the same order of magnitude as almost T independent $\chi(T)$ observed in f -moment-free pyrochlore iridates $\text{Eu}_2\text{Ir}_2\text{O}_7$. The CW temperature is found to be $\theta_{\text{CW}} = -19$ K, indicating antiferromagnetic interactions between Pr^{3+} moments. However, no anomalies or hysteresis, corresponding to the transitions to a long-range order or spin-glass, are observed down to 1.8 K.

Fig. 3 shows the magnetization curves $M(B)$ of $\text{Pr}_2\text{Ir}_2\text{O}_7$ measured at $T = 4.2$ K under fields up to 13 T along three

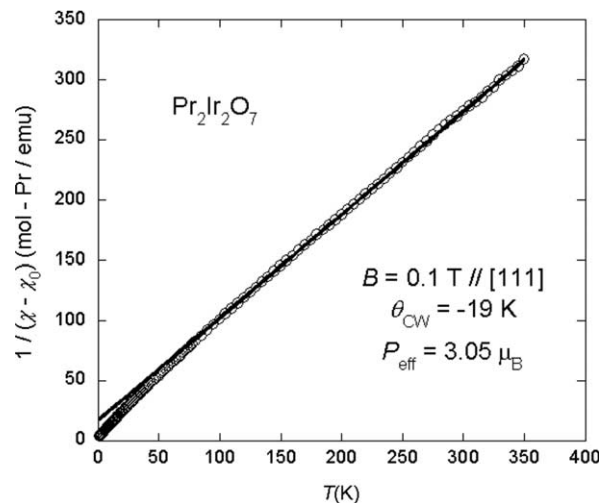


Fig. 2. Inverse susceptibility of $\text{Pr}_2\text{Ir}_2\text{O}_7$ single-crystal as a function of temperature between 1.8 and 350 K in a field of 0.1 T along the [111] direction. The solid line represents a fit to the Curie–Weiss (CW) law with a constant term to account for Ir 5d conduction electrons.

directions [100], [111] and [110]. As mentioned above, there exists Pauli paramagnetic contribution from the conduction 5d electrons, which can be estimated as $\chi_0 B$. The f -moment contribution can be estimated by subtracting $\chi_0 B$ from $M(B)$. $M - \chi_0 B$ exhibits significant field dependence and a tendency of saturation at $B = 13$ T. The magnetizations at 13 T along [100], [111] and [110] are close to the expected values for the [111] Ising anisotropy. The expected values for the [100] direction is $g_J J(1/\sqrt{3}) = 1.545 \mu_{\text{B}}/\text{Pr}^{3+}$ [two spins point in and two spins point out of each tetrahedron: Fig. 4(a)], for [111] direction, $g_J J(1 + 1/3 \times 3)/4 = 1.338 \mu_{\text{B}}/\text{Pr}^{3+}$ [three spins point in and one spin points out: Fig. 4(b)], and for [110] direction, $g_J J(\sqrt{2}/3 \times 2)/4 = 1.092 \mu_{\text{B}}/\text{Pr}^{3+}$ [one spin points in, one spin points out and two spins are free: Fig. 4(c)].

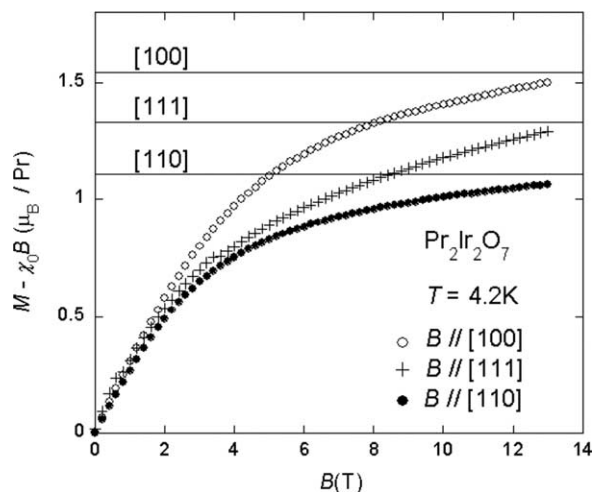


Fig. 3. Magnetization curves of $\text{Pr}_2\text{Ir}_2\text{O}_7$ single-crystal measured at $T = 4.2$ K along the three direction, [100], [111] and [110]. The horizontal lines show the saturation values calculated by assuming Ising anisotropy of each Pr^{3+} moment ($2.68 \mu_{\text{B}}$).

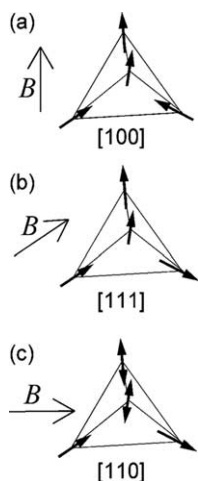


Fig. 4. Spin configurations with the magnetic field B along (a) $[100]$, (b) $[111]$ and (c) $[110]$ axes.

The magnetic part of the specific heat $C_m(T)$ is obtained by subtracting the lattice contribution from the total specific heat (not shown). The lattice part is estimated by the specific heat of metallic nonmagnetic iridate $\text{Eu}_2\text{Ir}_2\text{O}_7$, which is isostructural to $\text{Pr}_2\text{Ir}_2\text{O}_7$ [5]. By integrating $C_m(T)/T$, we find the magnetic entropy saturates to $R \ln(2)$ at around 20 K, which suggests that the ground state is a doublet.

In order to check the existence of the ground state doublet and the value of a magnetic moment precisely, we performed a powder inelastic neutron scattering experiments on $\text{Pr}_2\text{Ir}_2\text{O}_7$.

In the pyrochlore lattice, each Pr^{3+} ion is surrounded by eight O^{2-} ions forming a trigonally distorted cube of D_{3d} symmetry, with the electric principal axis along one of the local $\langle 111 \rangle$ directions. The crystal field with D_{3d} symmetry modifies the free-ion energy levels of Pr^{3+} ion, breaking up 9-fold degenerate $^3\text{H}_4$ ground multiplet into three singlets and three doublets.

Low-energy and high-energy inelastic neutron scattering data obtained at $T=5$ K (not shown) yield five peaks as a function of energy transfer due to the CEF excitation to each split level of $\text{Pr}^{3+} J=4$ multiplet. From the analysis of the neutron spectra, we determine the CEF energy level scheme for $\text{Pr}_2\text{Ir}_2\text{O}_7$ with the configuration of the ground state doublet, excited singlet levels at 162, 1218 and 1392 K, and excited doublet levels at 696 and 986 K. We find that Pr^{3+} ion has an isolated ground state doublet having a leading $|\pm 4\rangle$ component. The ground state doublet has the magnetic moment with a magnitude of $\sim 3.0 \mu_B$, consistent with the susceptibility. The g -tensors of the ground state doublet are anisotropic with only a g_{\perp} component along the local $\langle 111 \rangle$

direction with negligible g_{\parallel} component. This indicates that Pr^{3+} moments have Ising-like anisotropy along the local $\langle 111 \rangle$ direction for each Pr^{3+} ion. These are consistent with the results of the magnetization measurements of $\text{Pr}_2\text{Ir}_2\text{O}_7$. The fact that the ground state doublet is well-isolated from the excited levels is fortuitous; since even the first excited level is the nonmagnetic singlet, the complex CEF contribution is negligible at low temperature, and thus the magnetism below room temperature should solely come from the magnetic ground state doublet.

4. Conclusion

In conclusion, we have reported dc magnetic susceptibility, specific heat and inelastic neutron scattering measurements on the geometrically frustrated pyrochlore antiferromagnet $\text{Pr}_2\text{Ir}_2\text{O}_7$. We have found that the Pr^{3+} moments remain disordered down to 1.8 K. Our crystalline electric field calculation has indicated that the Pr^{3+} ground state is a well-isolated magnetic doublet that has Pr^{3+} Ising-like moments pointing along local the $\langle 111 \rangle$ directions of each tetrahedral unit.

Acknowledgements

We acknowledge T. Kamata for his technical support, and thank H. Tsunetsugu and S. Fujimoto for useful discussions. This work was supported in part by Grants-in-Aid for Scientific Research from JSPS and for the 21st Century COE 'Center for Diversity and Universality in Physics' from MEXT of Japan, and by the Inamori Foundation.

References

- [1] A.P. Ramirez, A. Hayashi, R.J. Cava, R. Siddharthan, B.S. Shastry, *Nature* 399 (1999) 333.
- [2] J.N. Reimers, J.E. Greedan, M. Bjorgvinsson, *Phys. Rev. B* 45 (1992) 7295.
- [3] J.S. Gardner, S.R. Dunsiger, B.D. Gaulin, M.J.P. Gingras, J.E. Greedan, R.F. Kiefl, M.D. Lumsden, W.A. MacFarlane, N.P. Raju, J.E. Sonier, I. Swainson, Z. Tun, *Phys. Rev. Lett.* 82 (1999) 1012.
- [4] J.S. Gardner, A. Keren, G. Ehlers, C. Stock, E. Segal, J.M. Roper, B. Fak, M.B. Stone, P.R. Hammar, D.H. Reich, B.D. Gaulin, *Phys. Rev. B* 68 (2003) 180401(R).
- [5] D. Yanagishima, Y. Maeno, *J. Phys. Soc. Jpn* 70 (2001) 2880.
- [6] S. Nakatsuji, Y. Machida, T. Tayama, T. Sakakibara, J. van Duijn, C. Broholm, R. Macaluso, J. Chan, Y. Maeno, (unpublished).

Monocrystal Elastic Constants of the Negative-Thermal-Expansion Compound Zirconium Tungstate (ZrW_2O_8)

F. R. Drymiotis, H. Ledbetter, J. B. Betts, T. Kimura, J. C. Lashley, and A. Migliori
Los Alamos National Laboratory, Los Alamos, New Mexico 87545, USA

A. Ramirez and G. Kowach
Lucent Technologies/Bell Laboratories, Murray Hill, New Jersey 07974, USA

J. Van Duijn
Johns Hopkins University, Baltimore, Maryland 21218, USA
(Received 26 January 2004; published 8 July 2004)

We measured zirconium tungstate's elastic constants C_{ij} . This compound shows relatively soft, nearly isotropic elastic constants with normal Poisson ratios and no approach to Born instability. ZrW_2O_8 shows normal ambient-temperature elastic constants C_{ij} , but remarkable dC_{ij}/dT that show dominant low-frequency acoustic-vibration modes. From the bulk modulus, we estimated the total ambient-temperature thermodynamic Grüneisen parameter as $\gamma = -1.2$. The dB/dT slope gives a Grüneisen parameter $\gamma = -7$. The 300–0 K bulk-modulus increase (40%) seems unprecedented and breaks Birch's law of corresponding states.

DOI: 10.1103/PhysRevLett.93.025502

PACS numbers: 62.20.Dc

Since the discovery in 1968 that zirconium-tungstate contracts when heated [1], much research ensued, both measurements and theories [2–7]. Zirconium tungstate represents perhaps the paradigm negative-thermal-expansion material: cubic crystal structure (thus, isotropic contraction), continued shrinking when heated over a wide temperature range (0–1050 K), a nearly constant thermal-expansivity coefficient $\beta = (1/V)(dV/dT)_P$, and (for oxides) large β .

Negative thermal expansion is attributed to lattice geometry: a large (44-atom) unit cell, interconnected Zr-O octahedra and W-O tetrahedra [8]. Zirconium tungstate's elastic constants C_{ij} assume importance for several reasons: (i) The C_{ij} reflect interatomic bonds, thus a check on interatomic potentials and assumptions about ionicity covalency. (ii) The bulk modulus $B = (C_{11} + 2C_{12})/3$ by high-pressure neutron diffraction [9] differs enormously from a theoretical estimate [10]. (iii) Some studies conclude that negative thermal expansion of a network structure implies a negative Poisson ratio [6]. (iv) Reported Debye or Einstein temperatures vary widely, and the C_{ij} provide a good estimate of these. (v) An accurate bulk modulus B gives a good estimate of the total thermodynamic Grüneisen parameter. (vi) The C_{ij}

provide a check on neutron-diffraction Born–von Karman force constants. (vii) From the C_{ij} , we can see whether any of the Born stability criteria accompany negative thermal expansion. (viii) The elastic-constant temperature derivatives dC_{ij}/dT relate directly to the Grüneisen parameter and to the equation of state.

Monocrystals were made using a nonequilibrium technique described elsewhere [2]. The specimen consisted of a (100)-oriented rectangular parallelepiped measuring 0.10 cm \times 0.16 cm \times 0.21 cm. From mass and volume, we estimated a 5.059-g/cm³ mass density, within about 0.5% of the x-ray density. For measurements, we used resonant-ultrasound spectroscopy [11].

For the C_{ij} , we found the results summarized in Table I. These give a (110) $[\bar{1}10]$ shear modulus $C' = (C_{11} - C_{12})/2 = 40.5$ GPa, a bulk modulus $B = (C_{11} + 2C_{12})/3 = 74.5$ GPa, and a Zener elastic anisotropy $A = C_{44}/C' = 0.677$. The 0.43% rms frequency measurement uncertainty means C_{ij} uncertainties of about 1%.

Figure 2 shows our results expressed as ratios $C_{ij}(T)/C_{ij}$ (300 K). Instead of C_{11} , C_{12} , and C_{44} , we show the more physical Zener elastic constants $C' = (C_{11} - C_{12})/2$, C_{44} , and $(C_{11} + 2C_{12})/3$, with the latter being the bulk modulus B . Because zirconium tungstate

TABLE I. Values of the monocrystal C_{ij} and the average-over-direction effective elastic constants: bulk modulus B , Young modulus E , shear modulus G , Poisson ratio ν , and Debye temperature calculated from the C_{ij} .

T (K)	C_{11} (GPa)	C_{12} (GPa)	C_{44} (GPa)	B (GPa)	E (GPa)	G (GPa)	ν	Θ_D
300	128.4	47.5	27.4	74.5	88.3	33.9	0.303	(321)
0	161.8	75.5	29.4	104.3	98.8	36.8	0.342	333

shows small elastic anisotropy, $C' = C_{44}$, for convenience we sometimes also invoke the shear modulus in Voigt's approximation, $G = (2C' + 3C_{44})/5$. Table I gives the monocrystal C_{ij} , the average-over-direction effective elastic constants, and the Debye temperature Θ_D calculated from the C_{ij} .

Compared with 17 other oxides [12], zirconium tungstate is relatively soft. Its bulk modulus B equals 53% of the average value. The effective shear modulus G is 44% of the average. (Here, we calculated G by Kröner's averaging method [13].) This relative softness reflects the crystal structure and the interatomic bonding. One view of zirconium tungstate's negative thermal expansion is that rigid ZrO_6 octahedra rotate toward or away from alignment with the unit-cell axes, altering the volume [14]. The softness to rotation appears in the bulk modulus, and more so in the shear modulus.

Our bulk-modulus result, $B = 74.5$ GPa, compares reasonably well with a high-pressure powder-specimen neutron-diffraction study: $B = 72.5$ GPa [9]. Both measurements refute a much-lower theoretical estimate [10]. A theoretical lattice-dynamics study [5] gave $B = 88.4$ GPa. This calculation included both ionic and covalent interatomic potentials. Below, we describe that our measured C_{ij} suggest a weak covalent component.

To characterize crystal elastic anisotropy, one usually invokes Zener's anisotropy definition [15]:

$$A = 2C_{44}/(C_{11} - C_{12}). \quad (1)$$

However, for materials with A less than unity (the present case), a better definition arises, as emphasized by Chung and Buessem [16]. These authors suggested

$$A^* = (G_V - G_R)/(G_V + G_R). \quad (2)$$

Here, G_V and G_R denote effective shear moduli calculated from the C_{ij} using Voigt or Reuss methods. For isotropic materials, $A^* = 0$. For a high-anisotropy material such as sodium, $A^* \approx 40$. For zirconium tungstate, $A^* = 0.02$, that is, nearly isotropic. With NiO and BaTiO_3 as exceptions, none of the oxides shown in Fig. 1 possess strong elastic anisotropy, and both exceptions are metastable.

Some studies [6] concluded that zirconium tungstate, because of its linkage crystal structure, may possess a negative Poisson ratio:

$$\nu_{ij} = -(S_{ij}/S_{ii}). \quad (3)$$

Here S_{ij} denotes the contracted S_{ijkl} tensor inverse of the C_{ijkl} . Because the material shows near elastic isotropy, we can consider the average-over-direction Poisson ratio, which relates to the bulk modulus B and effective shear modulus G :

$$\nu = (1/2)[(3B - 2G)/(3B + G)]. \quad (4)$$

The effective Poisson ratio equals 0.30, not only positive but also a value typifying many positive-thermal-

expansion materials. Thus, although many linkage-structure materials show negative Poisson ratios, zirconium tungstate does not.

To learn something about the interatomic bonding, we use a Blackman diagram [17,18], Fig. 1. In such a diagram showing reduced C_{ij} , materials with similar bonding cluster. Figure 1 shows that zirconium tungstate falls among the oxides, on the low C_{44}/C_{11} side, away from covalent compounds, which fall more in the center [18]. This location suggests a strong ionic contribution, and a weaker covalent contribution. Some lattice-dynamics calculations included both contributions [5], which would predict a stiffer material. Also, some studies suggested that negative thermal expansion requires high covalency [19]. If so, this covalency fails to affect the elastic constants. The Poisson ratio (0.30), being much higher than the ≈ 0.20 covalent limit [20], also suggests strong ionicity. On bonding, finally we note the small-moderate departure from the Cauchy condition $C_{12} = C_{44}$, a departure usually taken to indicate noncentral-force bonding. Again ZrW_2O_8 behaves similar to a typical oxide.

Some authors suggested elastic instabilities [5]. In Fig. 1, the Born instability conditions occur as lines $C_{12}/C_{11} = 1$ and $C_{44}/C_{11} = 0$. On this diagram, points move only slightly in response to changes in composition, temperature, and pressure. Thus, the zirconium-tungstate point occurs well away from mechanical instability.

From the C_{ij} , we can calculate an elastic Debye temperature Θ . At zero temperature Θ_{elastic} equals $\Theta_{\text{specific-heat}}$ [21]. To calculate Θ , we use the relationship

$$\Theta = (h/k)(3/4\pi V_a)^{1/3} \nu_m. \quad (5)$$

Here, h and k take their usual meanings, V_a denotes

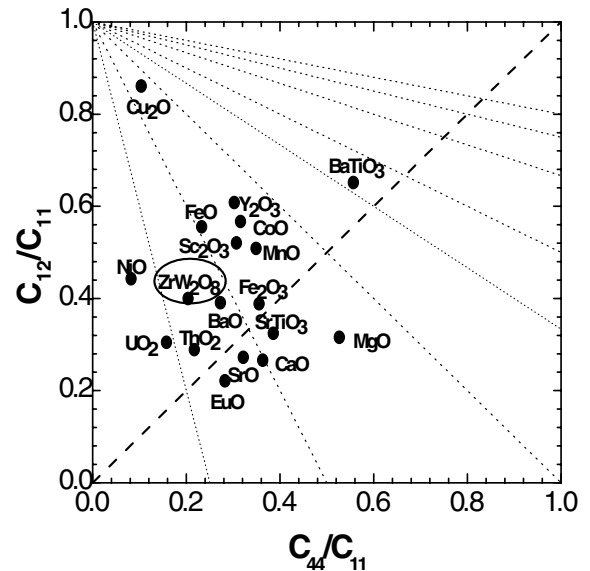


FIG. 1. Blackman diagram showing points for ZrW_2O_8 and seventeen other oxides. We see that ZrW_2O_8 looks normal.

atomic volume, and v_m denotes mean sound velocity, which we calculated from the C_{ij} using the Christoffel equations. For $T = 0$ K, we estimate $\Theta = 333 \pm 5$ K. Our result differs 7% from a recent specific-heat result: $\Theta = 311$ K [22].

Using the bulk modulus B , we can calculate the quintessential anharmonic-property parameter, the Grüneisen parameter:

$$\gamma = B_s \beta V / C_p. \quad (6)$$

Here β denotes volume thermal expansivity, V volume, and C_p heat capacity. For these properties we took $\beta = -26.4 \times 10^{-6} \text{ K}^{-1}$, $V(\text{unit cell}) = 767.22 \text{ \AA}^3$, $C_p = 207 \text{ J K}^{-1} \text{ mol}^{-1}$. Substitution gives the total thermodynamic (effective, average-over-mode) Grüneisen parameter $\gamma = -1.2$, consistent with several previous reports [3,22].

For a typical oxide such as CaO, in the temperature region 300 to 100 K, cooling increases the shear modulus about 5% and the bulk modulus about 4% [23]. From quasi-harmonic-model thermodynamics, the bulk-modulus temperature derivative has the form [24]

$$(\partial B_S / \partial T)_P = -\delta_S \beta B_S = -(\gamma + 1) \beta B_S. \quad (7)$$

Here S denotes entropy, P pressure, δ the second Grüneisen parameter, β the thermal expansivity $(1/V)(\partial V / \partial T)_P$, and γ the usual (first) Grüneisen parameter. For typical materials where γ ranges from 1 to 3, the derivative is usually negative. Indeed the measured $\partial B / \partial T$ provides a way to estimate γ . For zirconium tungstate, γ is negative and β is negative. Thus, from Eq. (7) one expects a negative $\partial B / \partial T$. Deriving an expression for the shear-modulus temperature dependence requires more assumptions. As an example, using Born's central-force near-neighbor-only face-centered-cubic model gives [25]

$$(\partial G / \partial T)_P = (9/28)(\partial B / \partial T)_P. \quad (8)$$

Taking a typical Poisson ratio, $\nu = 1/3$, then $G/B = 3/8$, and we obtain

$$(B/G)(\partial G / \partial T)(\partial B / \partial T) = 6/7. \quad (9)$$

So, approximately, in Born's model the relative shear-modulus change with temperature equals the relative bulk-modulus change. Born's model may apply fairly well to zirconium tungstate because central-interatomic-force potentials enjoyed some success [5] and because the ZrO_6 octahedra occupy fcc lattice positions [26].

Figure 2 presents three major surprises: (i) All the elastic constants stiffen during cooling, against the expectation that they should soften because the volume increases and the bulk modulus varies with volume as $B \propto V^{-4/3}$. (ii) The shear-modulus increase agrees with that of a typical oxide. (iii) The bulk modulus changes differently from the shear modulus. Indeed the bulk modulus

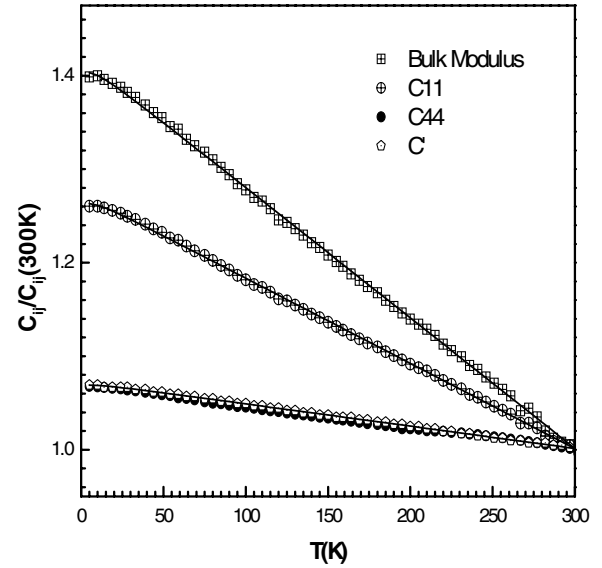


FIG. 2. Zirconium tungstate's normalized low-temperature elastic constants: bulk modulus B , C_{11} , C_{44} . Curves represent an Einstein-oscillator function. The bulk-modulus increase may be the largest ever reported. The near linearity to such low temperatures strongly suggests a low-frequency Einstein mode.

increases enormously. The 40% increase in the bulk modulus is unprecedented [27]. The increase breaks Birch's law of corresponding states: The bulk modulus depends on volume, not on how one changes volume—by temperature, pressure, composition, or phase transformation [28,29]. The Birch-law breakage provides strong evidence that the material's internal state changes during cooling. Another surprise is the near linearity to such low temperatures, or the low temperature at which the elastic constants begin to reflect strongly the zero-point energy. Also, we see unusual behavior in the Zener elastic anisotropy: $A = C_{44}/C'$ is essentially temperature invariant. Curiously, the bulk modulus extrapolates to zero near the material's decomposition temperature, 1050 K.

To the measurements in Fig. 2, we fit an expression based on the assumption that elastic stiffness decreases linearly with the thermal-oscillator-energy increase [30]:

$$C(T) = C_0 - s/(e^{t/T} - 1). \quad (10)$$

Here, C_0 denotes the zero-temperature elastic stiffness and t relates to the average Einstein temperature. Originally an adjustable parameter, in a quasi-harmonic Einstein-oscillator model, s becomes [31]

$$s = C_h - C_0 = 3kt\gamma(\gamma + 1)/V_a. \quad (11)$$

Here C_h denotes the harmonic zero-temperature elastic constant obtained by linear extrapolation from high temperatures, k is the Boltzmann constant, γ is the Grüneisen parameter, and V_a is the atomic volume. The high-temperature slope follows as

TABLE II. Einstein temperature calculated by fitting Eq. (10) to the $C_{ij}(T)$.

C_{ij}	C_{11}	C_{12}	C_{44}	C'	B
Θ_E (K)	26	23	17	34	25

$$dC/dT = -3k\gamma(\gamma + 1)/V_a. \quad (12)$$

Solving this relationship for γ and taking the negative root gives $\gamma = -7.0$, which differs sharply from the ambient-temperature value of $\gamma = -1.2$, and heads toward the large negative low-temperature values reported from thermal-expansion and specific-heat measurements [3,22].

The results of fitting Eq. (10) to the C_{ij} , and taking t to be an Einstein temperature Θ_E are summarized in Table II. For zirconium tungstate $t = 25 \text{ K} = 0.07\Theta_D$, enormously lower than expected.

The low values obtained for Θ_E reflect a dominant low-frequency acoustic-vibration mode. The lowest value of Θ_E appears for C_{44} , the (100) $[0kl]$ shear mode, and the highest Θ_E corresponds to $C' = (C_{11} - C_{12})/2$, the (110) $[\bar{1}10]$ shear mode. However, Θ_E shows remarkably low values for all modes, shear and dilational. These results agree with and confirm previous heat-capacity and phonon-density-of-states studies, which found low-frequency Einstein-type vibration modes.

Despite its peculiar anharmonic properties, zirconium tungstate possesses monocrystal elastic constants (harmonic properties) that present no surprises. Compared with other oxides, it is slightly soft, nearly isotropic, mechanically stable, and shows normal Poisson ratios. A Blackman diagram suggests strong ionic bonding. Its elastic-constant temperature derivatives (anharmonic properties) behave remarkably, perhaps uniquely, in both the magnitudes and the signs of the various dC_{ij}/dT . At a fundamental level, the C_{ij} - T behavior must relate to the remarkable negative-thermal-expansion behavior ZrW_2O_8 ; both depend on the Grüneisen parameter γ .

This research proceeded under the auspices of the National Science Foundation, the State of Florida, and the U.S. Department of Energy. J. Van Duijn also thanks DOE Grant No. DE-FG02-02ER45983 for support of this research.

[1] C. Martinek and F. Hummel, J. Am. Ceram. Soc. **51**, 227 (1968).

- [2] A. P. Ramirez and G. R. Kowach, Phys. Rev. Lett. **80**, 22 (1998).
- [3] G. Ernst, C. Broholm, G. Kowach, and A. Ramirez, Nature (London) **396**, 147 (1998).
- [4] T. Ravindran, A. Arora, and T. Mary, Phys. Rev. B **67**, 064301 (2003).
- [5] R. Mittal and S. Chaplot, Phys. Rev. B **60**, 7234 (1999).
- [6] D. Cao, F. Bridges, and A. Ramirez, Phys. Rev. B **68**, 014303 (2003).
- [7] J. Evans, W. David, and A. Sleight, Acta Crystallogr. Sect. B **55**, 333 (1999).
- [8] A. Sleight, Curr. Opin. Solid State Mater. Sci. **3**, 128 (1998).
- [9] J. Evans *et al.*, Science **275**, 61 (1997).
- [10] A. Pryde *et al.*, J. Phys. Condens. Matter **8**, 10 973 (1996); N. Allan *et al.*, Phys. Chem. Phys. **2**, 1099 (2000) challenged the validity of the interatomic potential used in this study.
- [11] A. Migliori and J. Sarrao, *Resonant Ultrasound Spectroscopy* (Wiley-Interscience, New York, 1997).
- [12] H. Ledbetter and S. Kim, in *Handbook of Elastic Properties of Solids, Liquids, and Gases* (Academic, San Diego, 2001), Vol. II, p. 65.
- [13] E. Kröner, Z. Phys. **151**, 504 (1958).
- [14] A. Pryde *et al.*, Phase Transit. **61**, 141 (1997).
- [15] C. Zener, *Elasticity and Anelasticity of Metals* (University of Chicago Press, Chicago, IL, 1948), p. 16.
- [16] D. Chung and W. Buessem, J. Appl. Phys. **38**, 2010 (1967).
- [17] M. Blackman, Proc. R. Soc. London **164**, 62 (1938).
- [18] H. Ledbetter, *Handbook of Elastic Properties of Solids, Liquids, and Gases* [Ref. [12], p. 57].
- [19] T. Mary, J. Evans, T. Vogt, and A. Sleight, Science **272**, 90 (1996).
- [20] H. Ledbetter and S. Kim, *Handbook of Elastic Properties of Solids, Liquids, and Gases* [Ref. [12], p. 281].
- [21] G. Leibfried and W. Ludwig, Solid State Phys. **12**, 275 (1961).
- [22] Y. Yamamura *et al.*, Phys. Rev. B **66**, 014301 (2002).
- [23] O. Anderson, *Equation of State of Solids* (Oxford, New York, 1995), p. 366.
- [24] E. Grüneisen, in *Handbuch der Physik* (Springer-Verlag, Berlin, 1926), p. 1, Eq. (46).
- [25] M. Gow, Proc. Cambridge Philos. Soc. **40**, 151 (1944).
- [26] M. Auray, M. Quarton, and M. Leblanc, Acta Crystallogr. Sect. C **51**, 2210 (1995).
- [27] A. Every and A. McCarty, in *Second and Higher Order Elastic Constants*, Landolt-Bornstein, New Series, Group III, Vol. 29a (Springer-Verlag, Berlin, 1992).
- [28] F. Birch, J. Geophys. Res. **66**, 2199 (1961).
- [29] F. Stacey, *Physics of the Earth* (Brookfield, Kenmore, Australia, 1992), p. 278.
- [30] Y. Varshni, Phys. Rev. B **2**, 3952 (1970).
- [31] H. Ledbetter, Phys. Status Solidi (b) **181**, 81 (1994).